HHS Public Access

Author manuscript

Cancer Lett. Author manuscript; available in PMC 2024 February 28.

Published in final edited form as:

Cancer Lett. 2023 February 28; 555: 216025. doi:10.1016/j.canlet.2022.216025.

Miz1 promotes KRAS-driven lung tumorigenesis by repressing the protocadherin Pcdh10

Jing Yang[1], **Changchun Hou**[1], **Huashan Wang**[1], **Edith A. Perez**[1], **Hanh Chi Do-Umehara**[1,‡], **Huali Dong**[1], **Vinothini Arunagiri**[1], **Fangjia Tong**[3], **Michelle Van Scoyk**[2], **Minsu Cho**[3], **Xinyi Liu**[3], **Xiaodong Ge**[4], **Robert A Winn**[2], **Karen M. Ridge**[5], **Xiaowei Wang**[3], **Navdeep S. Chandel**[5], **Jing Liu**[1,*]

[1]Department of Surgery, College of Medicine and University of Illinois Cancer Center, University of Illinois at Chicago, Chicago, IL 60612, USA

[2]Massey Cancer Center, Virginia Commonwealth University, Richmond, VA 23298, USA

[3]Department of Pharmacology and Regenerative Medicine and University of Illinois Cancer Center, University of Illinois at Chicago, Chicago, IL, USA

[4]Department of Pathology, University of Illinois at Chicago, 840 S. Wood St., Suite 130 CSN, MC 847, Chicago, IL 60612, USA

[5]Division of Pulmonary and Critical Care Medicine, Feinberg School of Medicine, Northwestern University, Chicago, IL 60611, USA.

Abstract

Targeting KRAS-mutated non-small-cell lung cancer (NSCLC) remains clinically challenging. Here we show that loss of function of Miz1 inhibits lung tumorigenesis in a mouse model of oncogenic KRAS-driven lung cancer. *In vitro*, knockout or silencing of Miz1 decreases cell proliferation, clonogenicity, migration, invasion, or anchorage-independent growth in mutant (MT) KRAS murine or human NSCLC cells but has unremarkable impact on non-tumorigenic cells or

*Correspondence should be addressed to Jing Liu (jinglius@uic.edu).

‡Current address: Division of Pulmonary and Critical Care Medicine, Feinberg School of Medicine, Northwestern University, Chicago, IL 60611, USA.

Author Contributions

J.Y., C.H., H.W., E.A.P., H.C.D., M.V.S., and M.C. performed experiments. R.A.W., K.M.R., X.W., and N.S.C. provided reagents and suggestions. J.L. contributed to manuscript preparation, hypothesis generation, and experimental design.

Competing Interests

Dr Liu's work has been funded by the NIH. The authors declare no potential competing interests.

Declaration of Interest Statement:

The authors declare no potential conflicts of interest.

CRediT author statement

Jing Yang: Conceptualization, Methodology, Formal analysis, Investigation, Visualization, Project administration **Changchun Hou, Huashan Wang, Edith A. Perez, Hanh Chi Do-Umehara, Huali Dong, Vinothini Arunagiri, Fangjia Tong, Michelle Van Scoyk, Xiaodong Ge:** Methodology, Formal analysis, Investigation, Visualization **Minsu Cho, Xinyi Liu**: Formal analysis **Robert A Winn, Karen M. Ridge, Xiaowei Wang, Navdeep S. Chandel:** Resources **Jing Liu:** Data Curation, Writing - Original Draft, Writing - Review & Editing, Supervision, Funding acquisition

wild-type (WT) KRAS human NSCLC cells. RNA-sequencing reveals Protocadherin-10 (Pcdh10) as the top upregulated gene by Miz1 knockout in MT KRAS murine lung tumor cells. Chromatin immunoprecipitation shows Miz1 binding on the *Pcdh10* promoter in MT KRAS lung tumor cells but not non-tumorigenic cells. Importantly, silencing of Pcdh10 rescues cell proliferation and clonogenicity in Miz1 knockout/knockdown MT KRAS murine or human tumor cells, and rescues allograft tumor growth of Miz1 knockout tumor cells *in vivo*. Miz1 is upregulated in MT KRAS lung tumor tissues compared with adjacent non-involved tissues in mice. Consistent with this, Miz1 is upregulated while Pcdh10 is downregulated in human lung adenocarcinomas (LUAD) compared with normal tissues, and high Miz1 levels or low Pcdh10 levels are associated with poor survival in lung cancer patients. Furthermore, the Miz1 signature is associated with worse survival in MT but not WT KRAS LUAD, and Pcdh10 is downregulated in MT compared to WT KRAS LUAD. Taken together, our studies implicate the Miz1/Pcdh10 axis in oncogenic KRAS-driven lung tumorigenesis.

Keywords

KRAS; non-small cell lung cancer; Pcdh10; gene regulation; Miz1

Introduction

Lung cancer is one of the most frequently diagnosed cancers and the leading cause of cancer-related mortality worldwide (3). Non-small-cell lung cancer (NSCLC) is the most common form of lung cancer, accounting for more than 85% of all lung cancers (4, 5). NSCLC comprises three main subtypes: lung adenocarcinoma (LUAD), which is the most common subtype of NSCLC in the U.S. making up 40% of lung cancer cases, squamous cell carcinoma, and large cell carcinoma. The predicted 5-year survival rate of NSCLC is estimated to be only 15.9%, a number that has been minimally improved in the past few decades (4, 5).

Activating mutations in Kirsten rat sarcoma viral oncogene homolog (KRAS) are the most prevalent oncogenic driver in NSCLC, occurring in 25–32% of patients with NSCLC (6, 7). The RAS superfamily (KRAS, NRAS and HRAS) is a protein superfamily of small GTPases that act as a binary switch in growth factor signaling. Upon stimulation by upstream growth factor receptors, RAS switches from the inactive (GDP-bound) form to the active (GTP-bound) form. This conformational change of RAS results in its interaction with and activation of several downstream effector pathways including the mitogen-activated protein kinase (MAPK) and phosphatidylinositol 3-kinase (PI3K) pathways, which execute programs related to cell cycle progression, differentiation, protein translation and evasion from cell death. Oncogenic RAS mutations are single base substitutions (most commonly affecting residues 12, 13 or 61) that lead to the stabilization of GTP binding and constitutive activation of RAS and downstream signaling cascades resulting in tumor cell growth (8–10). Despite significant efforts for decades, targeting KRAS-mutated NSCLS has proven to be clinically challenging (6, 11–13). Whereas direct therapeutic targeting of allele-specific KRAS(G12C) has recently been developed (12, 14), cancers driven by the other alleles of oncogenic KRAS remain difficult to treat. Although many small molecule inhibitors

targeting effector pathways downstream of KRAS have been developed (6, 15), many of these inhibitors activate feedback mechanisms that cause therapeutic resistance and concern for toxicity in the clinic (6, 13, 16–18). Alternative strategies aim at targeting codependent vulnerabilities or synthetic lethal partners that are essential in the context of oncogenic KRAS. KRAS activates multiple effector pathways that in turn mediate proliferation and survival signals. On the other hand, cancer cells must develop mechanisms to cope with mutant KRAS-induced oncogenic stress. These oncogenic signaling pathways and compensatory coping mechanisms lay the basis for synthetic lethal interactions (1, 2).

Myc interacting Zinc finger protein 1 (Miz1; also known as Zbtb17) belongs to the poxvirus and zinc-finger (19) domain/zinc finger transcription factor family. It has an amino-terminal POZ domain that is required for its transcriptional activity, and 13 zinc fingers at its carboxyl terminus (20, 21). Miz1 preferentially binds at the initiation region of a gene, and either activates gene transcription directly or represses gene transcription through interaction with other regulatory factors, such as Myc, Myc associated factor X (22), and B-cell lymphoma 6 protein (BCL-6), serving critical roles in cell proliferation, differentiation, cell-cycle progression and apoptosis (23–25). Whether Miz1 plays a role in lung cancer is not known. Here, we report that loss of function of Miz1 inhibits mutant (MT) KRAS lung tumor cell growth through upregulation of Pcdh10, leading to reduced lung tumorigenesis in oncogenic KRAS-driven NSCLC mouse model. Importantly, loss of function of Miz1 had marginal effect on normal cells or wild-type (WT) KRAS NSCLC cells. Our data suggest that Miz1 promotes tumorigenesis in MT KRAS NSCLC through repression of Pcdh10 and thus reveal therapeutic potentials. The clinical significance of our finding is supported by our observation that the Miz1 signature is associated with worse survival in MT but not WT KRAS LUAD, and Pcdh10 is downregulated in MT compared to WT KRAS LUAD.

Results

Loss of function of Miz1 inhibits tumor growth and progression in KRAS-driven mouse lung cancer model

KRAS mutations occur in 25–32% of NSCLC (6, 7), and concurrent inactivating mutations of the *TP53* tumor suppressor gene occur in about 50–70% of NSCLC (26). Codependency relationships between Miz1/Zbtb17 and KRAS and TP53 were identified (correlation scores 0.120 and −0.126, respectively) from The Cancer Dependency Map (DepMap), which comprises 990 human cancer cell lines through genome-scale CRISPR–Cas9 loss-of-function screening (Supplementary Table 1, highlighted in yellow). Additionally, codependency between Miz1/Zbtb17 and KRAS was observed only in MT KRAS cancer cells but not wild-type (WT) KRAS cancer cells (Supplementary Fig. 1A; left, WT KRAS: Pearson's correlation=0.05509, p=0.09; right, MT KRAS: Pearson's correlation=0.2139, p=0.0057). Furthermore, codependency between Miz1/Zbtb17 and TP53 loss was also observed only in MT KRAS but not WT KRAS lung cancer cells (Supplementary Fig. 1B; left, WT KRAS: Pearson's correlation=0.02390, p=0.8163; right, MT KRAS: Pearson's correlation=−0.3656, p=0.0283). These data indicate an implication of Miz1 in MT KRAS- and P53 loss-driven NSCLC.

To determine the role of Miz1 in NSCLC driven by MT KRAS and P53 loss, we used the $Kras^{LSL\text{-}G12D/+}Trp53^{fl/fl}$ mouse line as a mouse model of NSCLC, which carries a lox-stop-lox (LSL) sequence followed by the KRAS G12D point mutation allele as well as loxP sites flanking exons 2–10 of the transformation related protein 53 (Trp53) gene (referred to hereafter as KP mouse) (27) (28) (Supplementary Fig. 1C). Lung tumors were induced by intratracheal (i.t.) administration of adenoviruses encoding *Cre* recombinase (Ad/Cre) into KP mice as described (27) (Supplementary Fig. 1D). An empty adenoviral vector (Ad/null) was used as control. It has been reported that this mouse model of NSCLC mimics the genetic and histopathological features of the human disease (27). To determine the role of Miz1 in the development of lung cancer, we crossed KP mice to *Miz1*$(19)^{fl/fl}$ mice, in which the coding exons of the POZ domain of Miz1 that is required for its transcriptional activity were flanked by loxP sites (29) (referred to hereafter as KPM mice) (Supplementary Fig. 1C). We found that compared to Ad/Cre-treated KP mice, Ad/Cre-treated KPM mice had slower and reduced mortality rate and weight loss (Figs. 1A,B). We used longitudinal micro-computed tomography (micro-CT) to visualize and quantify the tumor mass (Supplementary Fig. 1E). Note, red indicated general chest areas; yellow indicated lung areas; and blue indicated healthy lung areas (Supplementary Fig. 1E). Longitudinal micro-CT showed that while Ad/null-treated KP and KPM mice had comparable healthy lung areas, Ad/Cre-treated KPM mice had more healthy lung areas (as indicated by blue areas) compared to Ad/Cre-treated KP mice (Fig. 1C). Quantification of tumor mass from longitudinal micro-CT revealed significantly reduced tumor loads from Ad/Cre-treated KPM mice compared to Ad/Cre-treated KP mice at 3- or 8-weeks after Ad/Cre administration (Fig. 1D). Accordingly, Ad/Cre-treated KPM mice had increased percentage of healthy lung areas than Ad/Cre-treated KP mice (Fig. 1E). To further confirm this, we used magnetic resonance imaging (MRI), which showed reduced tumor burden in Ad/Cre-treated KPM mice compared to Ad/Cre-treated KP mice (Fig. 1F), consistent with the results obtained from micro-CT. In accordance with the micro-CT and MRI data, whole lung histology revealed a decrease in tumor burden in Ad/Cre-treated KPM mice compared to Ad/Cre-treated KP mice at 3- or 8-weeks after Ad/Cre administration (Fig. 1G, Supplementary Fig. 1F). Sectional lung histology showed that at 3-weeks after Ad/Cre infection, KP mice had lesions of different stages of tumors in the lung, including atypical adenomatous hyperplasia (AAH), adenomas, and adenocarcinomas (30–32), while the lungs from KPM mice were mostly intact except sporadic AAH (Fig. 1H). At 8-weeks after Ad/Cre infection, tumors from KP mice progressed to more advanced adenocarcinomas, while KPM mice exhibited AAH and sporadic small adenomas (Fig. 1H). Lesions from KP mice had enlarged, pleomorphic nuclei or aberrant mitoses (arrows in Fig. 1H), or tumor giant cells (arrow heads in Fig. 1H), or exhibited nests of tumors cells surrounded by a desmoplastic stroma, indicating higher grade of tumors. To quantify the extent of progression of tumors, we employed a grading system as reported (32) to evaluate the stage of every tumor in each mouse using HALO (IndicaLab). We confirmed that loss of function of Miz1 resulted in markedly less severe tumor phenotype in Kras-driven lung cancer model: at 3-weeks after Ad/Cre infection, the lungs of KP mice contained lesions ranging from AAH to adenomas to low-grade adenocarcinomas, while the lungs of KPM mice only contained AAH (Fig. 1I); and at 8-weeks after Ad/Cre infection, tumors of KP mice progressed to higher grade of adenocarcinomas, while tumors of KPM mice had AAH,

small adenomas and low-grade adenocarcinomas (Fig. 1J). These data collectively indicate that loss of function of Miz1 suppresses lung tumor growth and progression.

Miz1 knockout reduces cell proliferation, clonogenicity, anchorage-independent growth, migration, and invasion in murine KRAS-MT lung tumor cells

We observed that Ad/Cre-treated KPM mice had reduced cell proliferation in the lung compared to Ad/Cre-treated KP mice, as analyzed by Ki67 staining and quantification using HALO (IndicaLab) (Fig. 2A,B). On the other hand, terminal deoxynucleotidyl transferase dUTP nick end labeling (TUNEL) staining showed a trend of increased apoptosis in the lung of Ad/Cre-treated KPM mice compared to Ad/Cre-treated KP mice (Fig. 2C). Multiple cells-of-origin have been reported in mouse lung adenocarcinoma derived from Cre recombinase-treated KP mice including alveolar epithelial type II cells (33–36). To investigate the mechanisms by which Miz1 promotes lung tumorigenesis, we used genetically defined mouse lung adenocarcinoma cells from Cre-induced tumors in KP mice (referred to hereafter as KP cells) as described (28, 37). We knocked out Miz1 in KP cells using the Crispr/Cas 9 system (Fig. 2D). Miz1 KO reduced cell proliferation in a time-dependent manner in KP cells, as analyzed by growth assay (Fig. 2E) and cell proliferation assay (MTS) (Fig. 2F). Miz1 KO decreased clonogenicity (Fig. 2G), migration (Fig. 2H), and invasion (Fig. 2I), as analyzed by colony formation assay and transwell migration/invasion assays. Soft agar assay further demonstrated that Miz1 KO inhibited the anchorage-independent growth of KP cells (Fig. 2J). Re-introduction of exogenous Miz1 using lentiviral vector into Miz1 KO KP cells (Miz1+ cells; Fig. 2K) reversed cell proliferation (Fig. 2L,M), colony formation (Fig. 2G), migration (Fig. 2H), and invasion (Fig. 2I). Similar results were obtained in additional two independent KO clones in KP cells with the Crispr/Cas 9 system (Supplementary Fig. 2A–L).

Silencing of Miz1 also reduces cell proliferation and clonogenicity in KRAS-MT human lung cancer cells

To determine whether Miz1 also plays a role in regulating cell proliferation and clonogenicity in KRAS-MT human lung cancer cells, we silenced *Miz1* in KRAS-MT lung epithelial adenocarcinoma cell lines A549, NCI-H23, and NCI-H2122 by stably expressing small hairpin RNA (shRNA) using lentiviral vector. Three different shRNAs targeting different sequences of *Miz1* all reduced cell proliferation in A549 cells, as analyzed by growth assay and MTS assay (Fig. 3A,B). The impact of different *Miz1* shRNAs on cell proliferation correlated with their efficiencies of *Miz1* silencing (Fig. 3A). Similar results were obtained in NCI-2122 (Fig. 3C) and NCI-H23 cells (Fig. 3D). Note, *Miz1* shRNA-1 (shMiz1-1) did not affect cell proliferation in NCI-H23 cells, most likely due to insufficient silencing of *Miz1* (Fig. 3D). We noticed that although the knockdown (KD) efficiency of shMiz1-1 seemed the same in A549 and NCI-H23 cells, its effect on cell proliferation was different between these cells. This indicates differential dose threshold effect of Miz1 on cell proliferation in these cells. Alternatively, different properties of KRAS mutations in different cell lines could attribute to differential dose effects. Note: A549 cells harbor KRAS (G12S) mutation while H23 cells harbor KRAS (G12C) mutation. On the other hand, stable overexpression of exogenous GFP-tagged Miz1 by lentiviral vector increased cell proliferation in NCI-H23 cells (Miz1 OE cells; Fig. 3E). Silencing of *Miz1* also reduced

colony-forming ability in A549 (Fig. 3F), NCI-H23 (Fig. 3G), and NCI-H2122 cells (Fig. 3H).

Development of therapies to directly target KRAS function has been challenging. Alternative strategies aim at targeting codependent vulnerabilities or synthetic lethal partners that are essential in the context of oncogenic KRAS. KRAS activates multiple effector pathways that in turn mediate proliferation and survival signals. On the other hand, cancer cells must develop mechanisms to cope with MT KRAS-induced oncogenic stress. These oncogenic signaling pathways and compensatory coping mechanisms lay the basis for synthetic lethal interactions (1, 2). We found that silencing of *Miz1* did not markedly affect cell proliferation in non-tumorigenic human bronchial epithelial BEAS-2B cells (Supplementary Fig. 3A–C). Intriguingly, silencing of *Miz1* did not reduce proliferation in WT KRAS NSCLC cell lines NCI-H1650 and NCI-H226 (Supplementary Fig. 3D,E). Rather, silencing of Miz1 increased proliferation in NCI-1650 cells (Supplementary Fig. 3D). This is in line with previous report that Miz1 inhibits cell proliferation in fibroblasts under physiological conditions (23). All together, these data suggest that Miz1 might promote tumorigenesis specifically in MT KRAS NSCLC. Whether loss of Miz1 confers synthetic lethality in KRAS MT NSCLC warrants future investigation.

Miz1 knockout or knockdown suppresses tumor growth in xenograft or allograft mouse models

As our data showed that Miz1 knockout (KO) in murine lung tumor KP cells or Miz1 knockdown (KD) in human NSCLC cells reduced cell proliferation and colony formation, we sought to determine whether these tumor cells with Miz1 KO or KD exhibited reduced tumor growth when transplanted into mice. Subcutaneous (s.c.) xenograft tumors derived from KP or NCI-H23 cells without or with Miz1 KO or KD were generated in athymic nude mice. Longitudinal measurement of tumor volume showed that tumor volume was significantly reduced in tumors derived from Miz1 KO KP cells compared to the control KP cells (Fig. 4A), associated with decreased tumor weight and tumor size (Fig. 4B,C). Re-introduction of exogenous Miz1 into Miz1 KO KP cells rescued the phenotype (Fig. 4D,E). Miz1 knockdown also resulted in a decrease in tumor volume of xenografts from NCI-H23 cells (Fig. 4F). To further confirm the role of Miz1 in promoting tumor growth in immunocompetent mice, we performed orthotopic lung transplantation in syngeneic mice by i.t. administration of the control KP cells or Miz1 KO KP cells into WT C57Bl6 mice, which have the same genetic background as KP mice from which KP cells were derived (28). Similar to Ad/Cre-treated KP and KPM mice, allografts from the control KP cells had tumors containing higher-grade adenocarcinomas, while allografts from Miz1 KO KP cells had tumors containing only small, low-grade adenomas (Fig. 4G). Again, re-introduction of exogenous Miz1 into Miz1 KO KP cells rescued the phenotype (Fig. 4G).

Pcdh10 is the top upregulated gene by Miz1 knockout in KRAS-mutant murine lung tumor cells

To investigate the mechanism by which Miz1 promotes KRAS-driven lung tumorigenesis, we first performed mass spectrometry (MS)-based quantitative proteomics in lung tissues from Ad/Cre-treated KP and KPM mice. We used the most stringent filter setting value

(5) for the minimum number of peptides, which is defined as the number of unique peptide sequences that match a given candidate protein. Gene set enrichment analyses (GSEA) revealed “apoptosis” as the second highest scoring gene set that was significantly upregulated in KPM mice compared to KP mice [Fig. 5A and Supplementary Table 2; Normalized Enrichment Score (NES)=1.7203728; nominal pvalue=0.006]. These data are in line with the observations that loss of Miz1 reduced cell proliferation and/or increased apoptosis *in vivo* and *in vitro* (Figs. 2,3). We then performed RNA-sequencing (RNA-seq) in 4 independent Miz1 KO KP cell clones together with 4 independent control KP cell clones. RNA-seq revealed 134 upregulated genes and 296 downregulated genes in Miz1 KO KP cells compared to the control KP cells [False Discovery Rate (FDR) < 0.05] (Fig. 5B and Supplementary Table 3). GSEA also revealed “apoptosis” as the enriched gene set upregulated in Miz1 KO KP cells compared to the control KP cells (Fig. 5C and Supplementary Table 4; NES=1.4508529; nominal pvalue=0.0). We first focused on the top 10 differentially expressed genes (FDR < 0.05): Protocadherin-10 (Pcdh10), Poly(ADP-Ribose) Polymerase Family Member 12 (Parp12), Calmin (Clmn), Transmembrane P24 Trafficking Protein Family Member 8 (Tmed8), Polypeptide N-Acetylgalactosaminyltransferase 12 (Galnt12), Tafa5 (also FAM19A5), Ankyrin Repeat And Sterile Alpha Motif Domain Containing 6 (Anks6), Spermatogenesis Associated 6 (Spata6), bone morphogenetic protein 7 (Bmp7), and zinc finger protein 704 (Zfp704) (Fig. 5D,E). The top upregulated gene Pcdh10 [$\log_2$(fold change)=11.5103; Q value=0.000264; n=4; Fig. 5E] belongs to the non-clustered protocadherin. Protocadherins are a subfamily of the cadherin superfamily that exhibit cell-to-cell adhesion activity with a mechanism thought to be distinct from that of classic cadherins. Pcdh10 has been proposed as a tumor suppressor gene involved in the regulation of growth control, cell invasion and metastasis in different types of cancers including gastric and colorectal cancers, as well as hematological malignancies (38). The role of Pcdh10 in lung cancer remains elusive except few reports showing downregulation of Pcdh10 by promoter methylation in NSCLC samples (39, 40). We noticed that Pcdh10 was undetectable in all 4 independent control KP cell clones but readily detected in all 4 Miz1 KO KP cell clones by RNA-seq (Fig. 5F). Note, mRNA expression of Pcdh10 (counts per million) in Fig. 5F was shown as unnormalized counts, different from those shown in Fig. 5D and 5E, which were normalized counts. We validated RNA-seq data using quantitative RT-PCR (qRT-PCR) with 6 clones of control and Miz1 KO KP cells (Fig. 5G). Additionally, re-introduction of exogenous Miz1 into Miz1 KO KP cells reversed Pcdh10 expression (Fig. 5H). Consistently, immunoblotting revealed that Pcdh10 protein was undetectable in the control KP cells but was apparent in Miz1 KO KP cells (Fig. 5I). Re-introduction of exogenous Miz1 into Miz1 KO KP cells reversed Pcdh10 protein expression comparable to the levels in the control KP cells (Fig. 5I). These data suggest a tight repression of Pcdh10 by Miz1 in the control KP cells. Silencing of Miz1 also drastically increased Pcdh10 mRNA expression in human A549, NCI-2122, and NCI-H23 cells (Fig. 5J). Consistently, Pcdh10 protein was barely detectable in the control A549 cells but was readily detected in Miz1 KD A549 cells (Fig. 5K), suggesting a general mechanism of Miz1-mediated repression of Pcdh10 in both mouse and human KRAS-mutant cells. We assessed Pcdh10 mRNA and protein expression in non-tumorigenic BEAS-2B cells without or with Miz1 KD. Intriguingly, silencing of Miz1 did not markedly alter Pcdh10 mRNA or protein expression in BEAS-2B cells (Supplementary Fig. 4A,B). Overexpression of Miz1

(Miz1 OE) did not affect Pcdh10 expression in BEAS-2B cells, either (Supplementary Fig. 4C). These data suggest that Pcdh10 might be subject to Miz1-mediated repression only in KRAS-mutant lung tumor cells but not in normal cells. These data are also in line with our observation that silencing of *Miz1* did not markedly affect cell proliferation in non-tumorigenic BEAS-2B cells (Supplementary Fig. 3A–C).

To determine whether Miz1 directly binds to the *Pcdh10* promoter to repress its transcription, we first determined whether mouse and human *Pcdh10* gene promoters contain consensus Miz1 binding motif YYAN-T/A-YYY ("(41)A[ctag][at](41)") (29). Using Sequence Manipulation Suite from http://www.bioinformatics.org/, we found both mouse and human *Pcdh10* gene promoters contain consensus Miz1 binding motif [−175 tcactccc −168 for mouse gene and −181 tcacactc −174 for human gene, relative to transcription start site (TSS)]. We then performed chromatin immunoprecipitation (ChIP) assay to determine whether Miz1 binds to the *Pcdh10* promoter. There was evidence of Miz1 enrichment on the *Pcdh10* promoter as compared to no-antibody (no Ab) control in the control KP cells (Fig. 5L). Similar results were obtained in Miz1 overexpression (Miz1 OE) human A549, NCI-2122, and NCI-H23 cells (Fig. 5M). These data suggest that Pcdh10 is a direct target for transcriptional repression by Miz1 in MT KRAS lung tumor cells. Intriguingly, when we queried our high-throughput ChIP sequencing (ChIP-seq) dataset from murine lung epithelial cell line MLE-12 cells under physiological conditions, we observed that Miz1 did not occupy the proximal *Pcdh10* promoter (Supplementary Fig. 4D). These data might provide a plausible explanation for our observation that Miz1 altered Pcdh10 expression in MT KRAS lung tumor cells but not in non-tumorigenic cells.

Silencing of Pcdh10 rescues cell proliferation and clonogenicity in Miz1-knockout or -knockdown KRAS-mutant mouse or human lung tumor cells

Now we have shown that loss of Miz1 reduces cell proliferation, clonogenicity, and ect., associated with substantial upregulation of Pcdh10. To determine whether loss of Miz1 inhibits cell proliferation and colony formation through upregulation of Pcdh10 in KRAS-mutant mouse lung tumor cells, we stably knocked down Pcdh10 using lentiviral vector in Miz1 KO KP cells. Silencing of Pcdh10 using three different Pcdh10 shRNAs with different targeting sequences restored cell proliferation and colony formation in Miz1 KO KP cells (Fig. 6A,B). We also stably silenced Pcdh10 in Miz1 KD human A549, NCI-H23, and NCI-2122 cells using lentiviral vectors expressing Pcdh10 shRNAs targeting different sequences of human Pcdh10. Similar to Pcdh10 KD in Miz1 KO KP cells, silencing of Pcdh10 also rescued cell proliferation and colony formation in Miz1 KD human NCI-H23 (Fig. 6C,D), A549 (Fig. 6E,F), or NCI-2122 cells (Fig. 6G,H). On the other hand, overexpression of Pcdh10 reduced cell proliferation in parental A549 cells (Supplementary Fig. 5A). Interestingly, overexpression of Pcdh10 did not affect cell proliferation in non-tumorigenic BEAS-2B cells (Supplementary Fig. 5B). Finally, silencing of Pcdh10 rescued growth of xenograft tumors derived from Miz1 KO KP cells (comparing Fig. 4A and Supplementary Fig. 5C). These data suggest that Pcdh10 at least in part mediates the inhibition of cell proliferation and colony formation by Miz1 deficiency in KRAS-mutant lung tumor cells.

Miz1 is upregulated in KRAS-mutant murine lung tumors and human NSCLC cell lines and primary tumors

Our data showed that Miz1 promotes KRAS-driven lung tumorigenesis. We sought to determine whether Miz1 expression is subject to regulation in the context of oncogenic KRAS-induced lung tumorigenesis. We observed that Miz1 protein was upregulated in tumors from Ad/Cre-treated $KRAS^{LSL\text{-}G12D/+}$ mice (Fig. 7A) or KP mice (Fig. 7B) compared to adjacent normal tissues, as analyzed by Miz1 immunohistochemistry (IHC). Quantification of Miz1 staining intensity using HALO (IndicaLab) revealed significantly increased staining in lung tumors compared to adjacent normal tissues from Ad/Cre-treated KP mice (Fig. 7C). Miz1 was also upregulated by MT KRAS in *ex vivo* AT2 cells isolated from KP mice upon Ad/Cre treatment (Fig. 7D). Miz1 mRNA and protein levels were also increased in a variety of NSCLC cell lines compared with primary normal human bronchial epithelial cells (HBEC) or non-tumorigenic BEAS-2B cells (Fig. 7E,F). Miz1 IHC of lung adenocarcinoma tissue microarray (TMA; Biomax: https://www.biomax.us/tissue-arrays/Lung/LC10013c), which contains 48 cases of lung adenocarcinomas and matched adjacent normal lung tissues, showed that Miz1 was markedly upregulated in lung adenocarcinomas compared to normal tissues (Fig. 7G). Note, A1~E8 were from 48 cases of lung adenocarcinomas and E9~J6 were from matched adjacent normal lung tissues, while J7-J10 were from non-related normal lung tissues and J11 was from adrenal gland; and H&E staining of the lung sections were shown side-by-side with Miz1 IHC images. Detailed sample information as well as enlarged H&E staining images of these samples are available at Biomax: https://www.biomax.us/tissue-arrays/Lung/LC10013c. Quantification of Miz1 staining of lung adenocarcinoma TMA using HALO (IndicaLab) revealed significantly increased staining in lung adenocarcinomas compared to matched normal tissues (Fig. 7H). Examples of Miz1 IHC staining of 3 lung adenocarcinomas and matched adjacent normal lung tissues from TMA (Fig. 7G) were shown, in which increased staining for Miz1 in lung tumors compared to the matched adjacent normal tissues was evident (Fig. 7I). To further support this, we also examined NSCLC samples with matched non-involved tissues from the cohort of our University of Illinois at Chicago (UIC) Medical Center. Similar results were obtained from the cohort of our UIC Medical Center (Fig. 7J,K; n=17). Note: in Fig. 7K, both normal and tumor tissues were shown, which revealed augmented Miz1 expression in tumor tissue compared to adjacent normal tissue. Collectively, our data show that oncogenic KRAS upregulates Miz1, which in turn represses Pcdh10, resulting in increased tumor cell proliferation and promotion of lung tumorigenesis (Fig. 7L).

TCGA database shows that Miz1 is upregulated while Pcdh10 is downregulated in lung adenocarcinomas, and high Miz1 levels or low Pcdh10 levels are associated with poor survival

Our data suggest that Miz1 promotes lung tumorigenesis at least in part through downregulation of Pcdh10. Consistent with this, Kaplan-Meier plots (K-M plots) revealed that high Miz1 level while low Pcdh10 level was associated with poor survival in lung cancer patients (Supplementary Fig. 6A,B). Furthermore, high Miz1/Pcdh10 ratio was associated with poor survival in lung cancer as revealed by K-M plots (Supplementary Fig. 6C). The Cancer Genome Atlas Lung Adenocarcinoma (**TCGA-LUAD**) database

showed increased Miz1 protein and mRNA levels (Supplementary Fig. 6D,E) while decreased Pcdh10 mRNA levels (Supplementary Fig. 6F, **left panel**) in lung adenocarcinoma compared to normal tissue. Further bioinformatic analysis of TCGA revealed 1) decreased expression of Pcdh10 in MT compared to WT KRAS LUAD (fold change=0.32; p=0.002) (Supplementary Fig. 6F, **right panel**; Supplementary Table 5); 2) a trend of association of high Pcdh10 level (Supplementary Fig. 6G) as well as high Pcdh10/Miz1 ratio (Supplementary Fig. 6H) with improved 5-year survival in MT but not WT KRAS LUAD. We did not observe an effect of Miz1 levels on prognosis in MT KRAS LUAD, probably due to limited sample size. These data indicate that the effect on prognosis is driven largely by Pcdh10 level while with less effect from the Miz1 level in MT KRAS LUAD, consistent with our interpretation that the major effect of Miz1 is to repress Pcdh10. Oncomine database (oncomine.org) also showed increased Miz1 mRNA levels while decreased Pcdh10 mRNA levels in lung adenocarcinomas compared to paired normal tissues in the cohort of *Selamat Lung* (Supplementary Fig. 6I,J). Increased Miz1 mRNA levels were also observed in NSCLC samples in the cohort of *Hou Lung* from the Oncomine database, including adenocarcinoma, squamous cell carcinoma, and large cell carcinoma, as compared to paired normal tissues (Supplementary Fig. 6K,L). The Oncomine analysis pipeline includes a comprehensive “molecular concepts” analysis, which encompasses diverse types of gene sets including those derived from Gene Ontology, KEGG, InterPro, as well as the Interactome analysis, which uses known components of the human protein interaction network as a framework for interpreting complex cancer signatures. Known protein-protein interactions are queried from The Human Protein Reference Database (HPRD). We observed that overexpression of Miz1 in lung tumors as compared to normal tissues was significantly associated with overexpression of known Miz1-interacting proteins identified by HPRD in the cohorts of *Selamat Lung*, *Hou Lung*, or *Landi Lung*, including host cell factor C1 (HCFC1), DNA Topoisomerase II Binding Protein 1 (TOPBP1), Msh Homeobox 2 (MSX2), General Transcription Factor IIi (GTF2I), Integrin β5 (ITGB5), or Myc proto-oncogene ($p < 0.05$) (Supplementary Fig. 6M–O), which we identified as the Miz1 signature associated with LUAD. Among them, overexpression of HCFC1, TOPBP1, MSX2, and GTF2I was significantly associated with overexpression of Miz1 in lung tumors in all of the three cohorts of *Selamat Lung*, *Hou Lung*, and *Landi Lung* (Supplementary Fig. 6M–O). Importantly, bioinformatic analysis of TCGA revealed association of the Miz1 signature with worse survival in MT but not WT KRAS LUAD (Fig. 7P). All together, these data further support the clinical relevance of Miz1 in lung cancer.

Discussion

Lung cancer is the leading cause of cancer-related death worldwide (3). NSCLC represents approximately 85% of lung cancer cases, with activating KRAS mutations being the most common of the oncogenic driver mutations (4, 5). However, there are not currently any approved therapies targeting KRAS. Our data suggest that oncogenic KRAS mutation induces upregulation of Miz1, which in turn promotes lung tumorigenesis through the repression of Pcdh10 expression.

Mass spectrometry-based quantitative proteomics and unbiased RNA-seq revealed the apoptosis pathway as one of the top enrichments by loss of (function of) Miz1 *in vivo*

and/or *in vitro*, which provides a plausible mechanism underlying reduced proliferation and/or increased apoptosis observed in Miz1 KO/KD cells and Miz1 MT mice. This notion is reinforced by the observation that silencing of Pcdh10, which has been reported to induce apoptosis and reduce proliferation (42) (43, 44), rescued Miz1 KO/KD phenotype. Besides apoptosis pathway, proteomics and RNA-seq also revealed enrichment in the other pathways, including myogenesis and bile acid metabolism by loss of (function of) Miz1. It's possible that there is mechanistic connection between apoptosis and the other pathways such as myogenesis/bile acid metabolism by loss of (function of) Miz1. We noticed that some common genes are indeed involved in both apoptosis and myogenesis, including glutathione peroxidase 3 (GPX3), spectrin alpha, non-erythrocytic 1 (SPTAN1), Clusterin (CLU), Gelsolin (GSN), amyloid precursor protein (APP) etc. On the other hand, it has been reported that apoptosis and bile acid metabolism are mechanistically connected (45). We do not exclude the possibility of the involvement of the other pathways, including myogenesis and bile acid metabolism, in Miz1-mediated regulation of lung tumorigenesis. For example, altered bile acid metabolism might contribute to apoptosis by Miz1 loss. Enrichment in the myogenesis pathway might contribute to reduced and delayed weight loss that is unproportionate to the tumor load in Miz1 MT mice in the mouse lung cancer model. Future investigation will determine the mechanistic connections between these pathways by loss of (function of) Miz1 in lung cancer.

Cadherins are calcium-dependent adhesion proteins that constitute a large family of cell adhesion molecules. Cadherins can be classified into several subfamilies: the classical cadherins, desmosomal cadherins, and protocadherins (PCDHs). The PCDH family can be further divided into two groups based on their genomic structure: clustered PCDHs (cPCDHs) and non-clustered PCDHs (ncPCDHs) (46, 47). Accumulating evidence implies that most ncPCDHs including Pcdh10 are tumor suppressive. Promoter methylation and transcriptional silencing of ncPCDH genes including Pcdh10 have been reported to occur in numerous epithelial cancer types and in multiple haematological malignancies, gliomas and medulloblastomas. Moreover, loss of expression of various ncPCDHs including Pcdh10 has been shown to correlate with poor prognosis or resistance in therapy. Furthermore, cancer-specific point mutations and deletions have also been demonstrated in several ncPCDH genes including Pcdh10. Pcdh10 is mutated in 14.81% of lung adenocarcinoma (https://portal.gdc.cancer.gov/genes/ENSG00000138650). Finally, ectopic expression of ncPCDHs into tumor cell lines bearing silenced PCDH genes reduced clonogenicity, anchorage-independent growth, and invasion *in vitro* as well as reduced xenograft growth in athymic mice (46, 47). Despite these extensive data indicating that ncPCDHs are potent tumor suppressors, the molecular mechanisms are unclear. Additionally, while Pcdh10 has been proposed as a tumor suppressor gene involved in the regulation of growth control, cell invasion and metastasis in different types of cancers including gastric and colorectal cancers, as well as hematological malignancies (38), the role of Pcdh10 in lung cancer remains elusive except few reports showing downregulation of Pcdh10 by promoter methylation in NSCLC samples (39, 40). Moreover, although in general the silenced ncPCDH genes including Pcdh10 can be experimentally reactivated by pharmacological DNA demethylation, for therapeutic purposes, there are concerns about off-target effects as demethylating agents usually target many different genes. Here, we identified Pcdh10

as a direct target for transcriptional repression by Miz1. We have previously reported that Miz1 represses gene transcription through epigenetic regulation (29). Further studies will investigate whether Miz1 is involved in promoter methylation and transcriptional silencing of Pcdh10 in NSCLC, which might reveal potential therapeutic target.

We show that loss of Miz1 markedly upregulates Pcdh10 expression in KRAS-MT mouse and human lung tumor cells while has minimal effect in non-tumorigenic BEAS-2B cells. Accordingly, loss of Miz1 reduces proliferation in tumor cells while has marginal effect in non-tumorigenic BEAS-2B cells. Miz1 occupies the *Pcdh10* promoter in MT KRAS lung tumor cells but not in normal lung epithelial cells. Future investigation is needed to elucidate the differential regulation of Pcdh10 by Miz1 in tumor cells versus non-tumorigenic cells. As Miz1 is upregulated by oncogenic KRAS, we speculate that supraphysiological levels of Miz1 invade low-affinity *Pcdh10* promoter in MT KRAS tumor cells. Nonetheless, Miz1 might represent a potential targeted therapy to specifically target cancer cells without affecting normal cells.

Despite decades of efforts, targeting KRAS-mutated NSCLC has proven clinically challenging. Alternative strategies aim at targeting codependent vulnerabilities or synthetic lethal partners that are essential in the context of oncogenic KRAS. Several lines of evidence linked the Miz1-Pcdh10 pathway to KRAS mutation. DepMap revealed increased codependency between Miz1 and KRAS in MT KRAS cancer cells compared to WT KRAS cancer cells. Further bioinformatic analysis of TCGA revealed 1) association of the Miz1 signature (Miz1 and its interacting proteins associated with lung adenocarcinoma) with worse survival in MT but not WT KRAS LUAD; 2) downregulation of Pcdh10 in MT compared to WT KRAS LUAD (fold change=0.32; p=0.002); and 3) a trend of association of high Pcdh10 level as well as high Pcdh10/Miz1 ratio with improved 5-year survival in MT but not WT KRAS LUAD. MT KRAS upregulates Miz1 in isolated mouse AT2 cells *ex vivo* and in the mouse lungs *in vivo*. Miz1 KO or KD reduced cell proliferation in KRAS-MT lung cancer cells but did not reduce cell proliferation in WT KRAS NSCLC NCI-H226 and NCI-H1650 cells or in non-tumorigenic cells. Whether loss of Miz1 confers synthetic lethality in KRAS MT NSCLC warrants future investigation. If it does, targeting Miz1 might provide a promising therapeutic target, as in principle, targeting synthetic lethal vulnerabilities in cancer should reduce the potential of side effects, because cells harboring the oncogenic mutation should have enhanced sensitivity to the perturbation than normal cells, which do not have the oncogenic mutation. Our data showed a connection of KRAS mutation to Miz1, however, whether Miz1 plays a role in the other NSCLC subtypes such as EGFR-mutant NSCLC needs further investigation.

Future studies are needed to determine the molecular mechanism by which Miz1 is upregulated in KRAS-driven NSCLC in mice and humans. We show that Miz1 mRNA and protein levels were higher in different NSCLC cell lines compared to normal human lung epithelial cell line BEAS-2B or human bronchial epithelial cell line (HBEC). However, the protein levels of Miz1 are not proportionate to its mRNA levels in different NSCLC cell lines. Additionally, TCGA database showed that while *Miz1* mRNA levels were modestly higher, its protein levels were drastically higher in lung adenocarcinomas compared to normal tissues, suggesting Miz1 might be upregulated

through both transcriptional and post-translational mechanisms. We showed that mutant KRAS upregulates Miz1 mRNA expression. TCGA showed significantly reduced promoter methylation of Miz1 in LUAD (http://ualcan.path.uab.edu/cgi-bin/TCGA-methyl-Result.pl?genenam=ZBTB17&ctype=LUAD). It will be interesting to investigate whether oncogenic KRAS results in reduced promoter methylation of Miz1 leading to its upregulation.

In summary, our study demonstrates that oncogenic activation of KRAS results in upregulation of Miz1, which in turn promotes tumor growth and progression through transcriptional repression of Pcdh10. The Miz1/Pcdh10 axis might be important in lung cancer as Miz1 expression is upregulated while Pcdh10 is downregulated in human lung adenocarcinomas, and high Miz1 level while low Pcdh10 level is associated with poor survival in lung cancer patients. Finally, Miz1 might represent a potential targeted therapy as targeting Miz1 has marginal effect on normal cells. We proposed here several potential strategies to target the Miz1 pathway therapeutically. We previously reported that the E3 ubiquitin ligase Mule (also known as Huwe1) targets Miz1 for ubiquitination-dependent proteasomal degradation (48). It has been reported that the cullin-E3 ligase family member CUL4B in turn targets Mule for ubiquitination and degradation (49, 50). These data suggest that inhibition of CUL4B may downregulate Miz1 protein via stabilizing Mule and facilitating Mule-mediated ubiquitination and degradation of Miz1. The small molecule inhibitor of CUL4B, MLN4924, is currently in Phase I clinical trials in patients with advanced solid tumors (51). On the other hand, we have reported that Serine 178 (Ser178) phosphorylation of Miz1 is required for its transcriptional repression function (52). We have identified potential kinase(s) that phosphorylates Miz1 at Ser178. Further investigation is needed to determine whether the kinase(s) is involved in NSCLC via regulating Miz1 function and if so, targeting the kinase(s) will provide potential therapeutic target(s). Alternatively, further investigation of the molecular mechanisms underlying the action of the Miz1 downstream effector(s) such as Pcdh10 to promote lung tumorigenesis will also reveal potential target(s).

Materials and Methods

Mice

Miz1(19)$^{fl/fl}$ mice on the C57BL/6 background have been described previously (29). *Lox-Stop-Lox KRAS*$^{G12D/+}$ *Tp53*$^{fl/fl}$ mice were described (28). Genotyping primers for Miz1(19)$^{fl/fl}$ mice: 5’-GTATTCTGCTGTGGGGCTATC-3’ and 5’-GGCTGTGCTGGGGGAAATC-3’; for *Lox-Stop-Lox KRAS*$^{G12D/+}$mice: 5’-CTAGCCACCATGGCTTGAGT-3’, 5’-ATGTCTTTCCCCAGCACAGT-3’, 5’-TCCGAATTCAGTGACTACAGATG-3’; *Tp53*$^{fl/fl}$ mice: 5’-GGTTAAACCCAGCTTGACCA-3’, 5’-GGAGGCAGAGACAGTTGGAG-3’. Wild-type C57BL/6 mice for orthotopic lung transplantation of KP cells were from The Jackson Laboratory (Strain: C57BL/6J; Stock: 000664). Athymic nude mice were from The Jackson Laboratory (Strain: Foxn1nu; Stock: 002019). The animal care and experiments were performed in compliance with the institutional and US National Institutes of Health guidelines and were approved by the Northwestern University Animal Care and Use Committee and the University of Illinois at Chicago Animal Care Committee.

Mouse model of KRAS-driven NSCLC

Lung tumors were induced by intratracheal inhalation of 10^9 PFUs of adenoviral Cre recombinase into KP or KPM mice (ViraQuest), as previously described (27) (28).

Xenograft or allograft mouse models of lung cancer

Xenograft tumors were induced by subcutaneous (s.c.) injection of KP or NCI-H23 cells (2×10^6 in 100 μl saline) without or with Miz1 KO or KD into the right flank of female athymic nude mice (female; 4–5 weeks old). Allograft tumors were injected by intratracheal (i.t.) instillation of (4×10^6 cells in 50 μl saline) KP cells into C57BL/6 mice (female; 9–10 weeks old).

Antibodies for Western Blot

GFP antibody (3E6, Thermo Fisher Scientific; 1:500 dilution); Miz-1 antibody (D7E8B, Cell Signaling Technology; 1:500 dilution) to detect human Miz1 proteins; Miz-1 antibody (PA5-67999, Thermo Fisher Scientific; 1:500 dilution) to detect mouse Miz1 proteins; Vinculin antibody (MA5-11690, Invitrogen; 1:2000 dilution); β-actin antibody (A5441, Sigma-Aldrich; 1:20,000 dilution). Pcdh10 antibody (Cat #21859-1-AP; Thermo Fisher Scientific; 1:500 dilution).

Micro-CT scan

In vivo mouse lung micro-CT scans were conducted with the subjects anesthetized with 1.5–2% isoflurane in 100% oxygen. Micro-CT datasets were acquired on a dedicated small animal micro-PET/CT scanner (NanoScan8 MEdiso, Budapest Hungary). Scan parameters were as follows: 50-kVp X-ray source voltage, 320-ms exposure time/projection, 720 projections with a field of view (FOV) ~ 1–2 cm covering the lung. Total acquisition time ~ 4 minutes, yielding three-dimensional datasets with isotropic voxel size of 250 micrometers, corresponding to four different phases of the breathing cycle (4D).

Histological analysis

Tissue samples were fixed in 4% paraformaldehyde (24 h), processed and embedded in paraffin. Sections (5 μm) were prepared and mounted on coverslips for staining with haematoxylin and eosin, and tissue images were captured using Nikon ECLIPSE E800, or using the TissueGnostics Tissue/Cell High Throughput Imaging Analysis System (Vienna, Austria) and TissueFAXS software (TissueGnostics, Los Angeles, CA) at the Northwestern University Cell Imaging Facility.

Immunohistochemistry (IHC) staining

Mouse and human lung tissues were fixed in 4% paraformaldehyde (24 h), processed and embedded in paraffin. TUNEL staining was performed by the Northwestern University Mouse Histology and Phenotyping Laboratory in deparaffinized slides using the ApopTag® Peroxidase In Situ Apoptosis Detection Kit (S71000; EMD Millipore). For IHC of Miz1 and Ki67, briefly, deparaffinized slides were incubated with Miz1 antibody (ab121232, Abcam; 1:500) or Ki67 antibody (TEC-3, Dako; 1:50) overnight at 4 degrees. Nonimmune rabbit or rat IgGs (Abcam) were used as negative controls. Detection was performed with

the biotin-streptavidin peroxidase system (Vector Lab). Nuclei were visualized with 4′,6-diamidine-2-phenylindole (DAPI). Positive stain shows brown/dark brown and the nuclei are stained blue. Formalin-fixed paraffin-embedded (FFPE) tissues of NSCLC from the UIC Medical Center were from UIC lung cancer Biorepository.

Stable KO or KD or OE cell lines

Stable Miz1 KO KP cells were generated in parental KP cells using lentiviral Crispr/Cas 9 system and single guide RNA (gRNA) accordingly to the protocol of Feng Zhang's laboratory (https://www.addgene.org/crispr/zhang/#gecko) (53). gRNA target sequences: AGAACATCGTCCACGTTCTC or GAGCCTTAGCCCTGAGAACG. gRNA was cloned into lentiCrisprV2 plasmid, which was co-transfected with VSV-G plasmid (Addgene, # 12259) and psPAX2 plasmid (Addgene, # 12260) into HEK 293T cells at the ratio of 500 ng:250ng:250ng. Forty-eight hours later, the supernatants containing packaged lentiviruses were collected and used to transduce KP cells, which were then selected using puromycin (1.6 μg/ml). Single clones were picked up and KO clones were confirmed by western blotting. Exogenous mouse Miz1 was re-introduced back to Miz1 KO KP cells with lentiviral vectors expressing mouse Miz1 generated by The DNA/RNA Delivery Core of Skin Disease Research Core Center. Stable Miz1 KD cell lines were generated in A549/NCI-H23/NCI-2122 cells with SMARTvector Lentiviral shRNAs targeting human Miz1 (V3SVHS02_8619648, V3SVHS02_4756503, V3SVHS02_10078083; Horizon Discovery) or non-targeting control (Cat # S02-005000-01; Horizon Discovery) according to the manufacturer's instructions and selected with puromycin (0.5 μg/ml). Stable Pcdh10 KD cell lines were generated in Miz1 KO KP and Miz1 KD A549/NCI-H23/NCI-2122 cells with SMARTvector Lentiviral shRNAs targeting mouse or human Pcdh10 (mouse: V3SVMM10_14394290, V3SVMM10_13008158, V3SVMM10_15986705; human: V3SVHS09_7727626, V3SVHS09_5829235, V3SVHS09_6105808; Horizon Discovery) or non-targeting control (mouse: Cat # S10-005000-01; human: Cat # S09-005000-01; Horizon Discovery). Stable Miz1 or Pcdh10 overexpressing cell lines were generated in A549/NCI-H23/NCI-2122/BEAS-2B cells using lentiviral vectors expressing human Miz1 or Pcdh10 with a C-terminal mTagGFP (Cat # RC216143L4V for Miz1 or RC2145242L4V for Pcdh10; Origene) or empty lentiviral vector control (Cat # PS100093V; Origene) and selected with puromycin (0.5 μg/ml).

Chromatin immunoprecipitation (ChIP) assays

Cells were cross-linked with EGS (25mM) for 20 min, then fixed with 1% formaldehyde for 10 min. Glycine (1M, dissolved in PBS) was used to quench the fixation. Cells were then lysed with ChIP SDS Lysis Buffer (Millipore, Catalog # 20-163) with protease inhibitors (100mM PMSF, 10 mM PNPP, 1 mM Na3VO4; 1 mM DTT, 1 μg/mL Aprotinin). Lysates were subjected to sonication on ice to shear DNA to fragments between 200 and 500 base pairs. Sonication efficiency was examined using 1% agarose gel electrophoresis. 50μg sonicated DNA was used for immunoprecipitation without or with specific antibody (1–2μg). For KP cells, Miz1 antibody (sc-136985 X; Santa Cruz Biotechnology) was used. For stable human Miz1-overexpressing A549/NCI-H23/NCI-2122 cells, GFP antibody (3E6; Thermo Fisher Scientific) was used. Precipitated DNA-beads complex was washed with Low Salt Immune Complex Wash Buffer (Catalog # 20-154), High Salt Immune Complex

Wash Buffer (Catalog # 20-155), and LiCl Immune Complex Wash Buffer (Catalog # 20-156) twice, TE Buffer (Catalog # 20-157) twice. Eluted DNA was purified and subjected to qPCR with primers corresponding to the predicted Miz1-binding motif of the *Pcdh10* promoter. Enrichment was calculated as qPCR values from antibody-precipitated ChIP DNA normalized to no-antibody ChIP DNA. Primer sequences: For mouse Pcdh10: 5'GGCTGTTCTTGCTCTCACAC3', 5'CCCAATGCTTGTGATCTCGG3'; For human Pcdh10: 5'AACTTTCCGCGGCATTGTC3', 5'CCCTCATTCTGCCAACCAAT3'. ChIP-seq was performed and analyzed as we previously reported (54). Briefly, DNA samples were quantitated by qubit and sequencing libraries were generated using an Illumina TruSEQ based protocol. Libraries were sequenced on an Illumina NovaSEQ6000 (100 bp, paired-end) at University of Chicago Genomics Facility and the raw sequencing data were demultiplexed using the Illumina bcl2fastq software. Sequencing raw reads were aligned to the mouse genome mm10 using BWA MEM. Apparent PCR duplicates were removed using Picard MarkDuplicates to ensure that downstream results were not biased by PCR duplication artifacts. Peaks were called against inputs using Macs2; normalized bedgraph tracks were generated using the --SPMR flag, and converted to bigWig using UCSC tool bedGraphToBigWig.

RNA-seq

RNA-seq of the control KP or Miz1 KO KP cells was performed by University of Chicago Genomics Facility. Briefly, Total RNA was extracted and purified using NucleoSpin RNA kit. RNA quantity and quality were assessed using the Agilent Bio-analyzer. Stranded oligo-dT-based NGS libraries were generated using the Illumina stranded mRNA library kit. Indexed sequence libraries were pooled for multiplexing, and paired-end sequencing (100 bp) were performed on NovaSEQ6000 using dual-index sequencing primers (Illumina). Reads were aligned using TopHat2 to the mm10 reference genome, and differential expression was assessed using edgeR, which was performed by Research Informatics Core, Research Resources Center, University of Illinois at Chicago. Enrichment analysis was performed using curated databases including Gene Ontology (GO) or KEGG PATHWAY mapping.

Quantitative PCR

Quantitative PCR (qPCR) was performed using iQ™ SYBR® Green Supermix (BIO-RAD) on a CFX Connect™ Real-Time PCR Dection System (BIO-RAD). For qRT-PCR, total RNA was extracted from cells by NucleoSpin RNA kit (Macherey-Nagel), followed by cDNA synthesis v phosphoribosyltransferse (HPRT) for mouse genes and glyceraldehyde 3-phosphate dehydrogenase (GAPDH) for human genes. Primer sequences: For mouse Pcdh10: 5' ACGAGCGCCTTACAAACCAC3', 5'CGTTAAATGAGCCTCTCCACGC3'; For human Pcdh10: 5'ACAAACCACCATATTTGACACGGA3', 5'GCTTTTGTTGGTCGACTTTGTGC3'; For human Miz1: 5'GGGCAGGTGCTGGAGTTTAT3', 5'AACAGGGCAGACCTTCTGTG3'; For mouse HPRT: 5'AGGCCAGACTTTGTTGGATTTGAA3' and 5'CAACTTGCGCTCATCTTAGGCTTT3'; For human GAPDH: 5'GAAGGTGAAGGTCGGAGTC3' and 5'GAAGATGGTGATGGGATTTC3'.

Cell growth and MTS assay

For 6-day growth assay, cells were seeded at the concentration of 15000–25000 cells/well in 24-well cell culture plate. Cells were trypsinized and counted using hemocytometer for consecutive 6 days. For MTS assay, cells were seeded at the concentration of 500–1000 cells/well in 96-well cell culture plate in triplicates. Cell proliferation was determined with CellTiter 96® AQ_{ueous} One Solution Cell Proliferation Assay (MTS) (Cat # G3582, Promega). The absorbance at 490nm (OD490) was recorded using the SpectraMax 340PC384 Microplate Reader (Molecular Devices) at 24, 48, and 72 h.

Clonogenic Assay

Cells were seeded at the concentration of 1000 cells/well in 12-well cell culture plate in triplicates. When cells were confluent (usually at 6–7 day), cells were stained with 1mL crystal violet (250mg Crystal Violet, 6mL Gluteraldehyde, 44mL dd H2O). The number of colonies were viewed and counted using ImageJ and Quantity-one software.

Soft agar assay

Cells (5000 per well) were mixed with 0.6% noble agar in growth medium, plated on top of a solidified layer of 1% noble agar in growth medium, in a 6-well plate in triplicates, and fed every 3 d with growth medium. After 3–4 weeks, pictures were taken and the number of the colonies were counted using metamorph.

Transwell migration and invasion assays

For migration assays, 8.0μm pore size/24-well format cell culture inserts (BD353097, BD) were used. For invasion assays, 8.0μm pore size/24-well format, growth factor reduced Matrigel invasion chambers were used (BD354483, BD). Cells were seeded at 15,000–30,000 cells/well in the inserts/chambers with DMEM plus 1% FBS. Normal DMEM medium with 10% FBS was distributed in each well. At 24 h at 37 °C, inserts/chambers were gently picked up before a brief PBS rinse and 0.05% crystal violet coloration. Cells at the bottom position of the inserts/chambers were photographed and counted with Evos FL Auto II Imager and Image J.

TCGA Data

mRNA and/or protein expression was obtained for the TCGA Lung adenocarcinoma (LUAD) through UALCAN (http://ualcan.path.uab.edu/index.html). Transcripts Per Million (TPM) values were used for mRNA expression, while log-transformed Z-values for protein expression.

Kaplan–Meier (22) plotter

Kaplan–Meier survival plots with logrank *P* values were provided from KM Plotter (http://kmplot.com) (56). The clinical information was provided from this website. Gene expression data and the survival information were derived from integrated databases including GEO, EGA, and TCGA. The patient samples are divided into two groups to evaluate the prognostic value of a particular gene based on quantile expressions, and the Kaplan–Meier survival plot is generated by these two groups of patient cohorts.

Isolation of AT2 cells *ex vivo* and treatment with Ad/Cre

AT2 were isolated using antibody-based affinity purification with CD45 negative selection and EpCAM positive selection, followed by Ad/null or Ad/Cre infection as we previously described (52).

Statistical analysis

Data were analyzed using an unpaired Student's *t*-test, with the assumption of normal distribution with equal variance and n indicating biological replicates.

Supplementary Material

Refer to Web version on PubMed Central for supplementary material.

Acknowledgements

We thank the Cardiovascular Research Core at the University of Illinois at Chicago for the services. We thank Pieter W. Faber and Sandhiya Arun (University of Chicago Genomics Facility) for performing RNA-seq and scRNA-seq. We thank Zhengdeng Lei, Pinal Kanabar, Melline Fontes Noronha, and Mark Maienschein-Cline (Research Informatics Core, Research Resources Center, University of Illinois at Chicago) for the RNA-seq and scRNA-seq analyses. We thank Yale MS & Proteomics Resource for performing the proteomics. JL is supported by the US National Institutes of Health (HL141459 to J.L.).

Data Availability Statement

All data generated or analyzed during this study are included in this published article [and its supplementary information files].

References

1. Kim J et al. , XPO1-dependent nuclear export is a druggable vulnerability in KRAS-mutant lung cancer. Nature 538, 114–117 (2016). [PubMed: 27680702]
2. Aguirre AJ, Hahn WC, Synthetic Lethal Vulnerabilities in KRAS-Mutant Cancers. Cold Spring Harb Perspect Med 8 (2018).
3. Herbst RS, Heymach JV, Lippman SM, Lung cancer. N Engl J Med 359, 1367–1380 (2008). [PubMed: 18815398]
4. Chen Z, Fillmore CM, Hammerman PS, Kim CF, Wong KK, Non-small-cell lung cancers: a heterogeneous set of diseases. Nat Rev Cancer 14, 535–546 (2014). [PubMed: 25056707]
5. Gridelli C et al. , Non-small-cell lung cancer. Nat Rev Dis Primers 1, 15009 (2015). [PubMed: 27188576]
6. Moore AR, Rosenberg SC, McCormick F, Malek S, RAS-targeted therapies: is the undruggable drugged? Nat Rev Drug Discov 19, 533–552 (2020). [PubMed: 32528145]
7. Mitsuuchi Y, Testa JR, Cytogenetics and molecular genetics of lung cancer. Am J Med Genet 115, 183–188 (2002). [PubMed: 12407699]
8. Li S, Balmain A, Counter CM, A model for RAS mutation patterns in cancers: finding the sweet spot. Nat Rev Cancer 18, 767–777 (2018). [PubMed: 30420765]
9. Pylayeva-Gupta Y, Grabocka E, Bar-Sagi D, RAS oncogenes: weaving a tumorigenic web. Nat Rev Cancer 11, 761–774 (2011). [PubMed: 21993244]
10. Malumbres M, Barbacid M, RAS oncogenes: the first 30 years. Nat Rev Cancer 3, 459–465 (2003). [PubMed: 12778136]

11. Camidge DR, Doebele RC, Kerr KM, Comparing and contrasting predictive biomarkers for immunotherapy and targeted therapy of NSCLC. Nat Rev Clin Oncol 16, 341–355 (2019). [PubMed: 30718843]
12. Mullard A, Cracking KRAS. Nat Rev Drug Discov 18, 887–891 (2019). [PubMed: 31780856]
13. Rotow J, Bivona TG, Understanding and targeting resistance mechanisms in NSCLC. Nat Rev Cancer 17, 637–658 (2017). [PubMed: 29068003]
14. Ostrem JM, Peters U, Sos ML, Wells JA, Shokat KM, K-Ras(G12C) inhibitors allosterically control GTP affinity and effector interactions. Nature 503, 548–551 (2013). [PubMed: 24256730]
15. Baines AT, Xu D, Der CJ, Inhibition of Ras for cancer treatment: the search continues. Future Med Chem 3, 1787–1808 (2011). [PubMed: 22004085]
16. Samatar AA, Poulikakos PI, Targeting RAS-ERK signalling in cancer: promises and challenges. Nat Rev Drug Discov 13, 928–942 (2014). [PubMed: 25435214]
17. Ryan MB, Corcoran RB, Therapeutic strategies to target RAS-mutant cancers. Nat Rev Clin Oncol 15, 709–720 (2018). [PubMed: 30275515]
18. Dang CV, Reddy EP, Shokat KM, Soucek L, Drugging the 'undruggable' cancer targets. Nat Rev Cancer 17, 502–508 (2017). [PubMed: 28643779]
19. Monteil V et al. , Inhibition of SARS-CoV-2 Infections in Engineered Human Tissues Using Clinical-Grade Soluble Human ACE2. Cell 181, 905–913.e907 (2020). [PubMed: 32333836]
20. Wanzel M, Herold S, Eilers M, Transcriptional repression by Myc. Trends Cell Biol 13, 146–150 (2003). [PubMed: 12628347]
21. Peukert K et al. , An alternative pathway for gene regulation by Myc. Embo j 16, 5672–5686 (1997). [PubMed: 9312026]
22. Riva L et al. , Discovery of SARS-CoV-2 antiviral drugs through large-scale compound repurposing. Nature 586, 113–119 (2020). [PubMed: 32707573]
23. Herold S et al. , Negative regulation of the mammalian UV response by Myc through association with Miz-1. Mol Cell 10, 509–521 (2002). [PubMed: 12408820]
24. Saito M et al. , BCL6 suppression of BCL2 via Miz1 and its disruption in diffuse large B cell lymphoma. Proceedings of the National Academy of Sciences of the United States of America 106, 11294–11299 (2009). [PubMed: 19549844]
25. Si J, Yu X, Zhang Y, DeWille JW, Myc interacts with Max and Miz1 to repress C/EBPdelta promoter activity and gene expression. Molecular cancer 9, 92 (2010). [PubMed: 20426839]
26. Takahashi T et al. , p53: a frequent target for genetic abnormalities in lung cancer. Science 246, 491–494 (1989). [PubMed: 2554494]
27. DuPage M, Dooley AL, Jacks T, Conditional mouse lung cancer models using adenoviral or lentiviral delivery of Cre recombinase. Nat Protoc 4, 1064–1072 (2009). [PubMed: 19561589]
28. Glasauer A, Sena LA, Diebold LP, Mazar AP, Chandel NS, Targeting SOD1 reduces experimental non–small-cell lung cancer. J Clin Invest 124, 117–128 (2014). [PubMed: 24292713]
29. Do-Umehara HC et al. , Suppression of inflammation and acute lung injury by Miz1 via repression of C/EBP-delta. Nature immunology 14, 461–469 (2013). [PubMed: 23525087]
30. Jackson EL et al. , Analysis of lung tumor initiation and progression using conditional expression of oncogenic K-ras. Genes Dev 15, 3243–3248 (2001). [PubMed: 11751630]
31. Jin C et al. , Commensal Microbiota Promote Lung Cancer Development via γδ T Cells. Cell 176, 998–1013.e1016 (2019). [PubMed: 30712876]
32. Jackson EL et al. , The differential effects of mutant p53 alleles on advanced murine lung cancer. Cancer Res 65, 10280–10288 (2005). [PubMed: 16288016]
33. Xu X et al. , Evidence for type II cells as cells of origin of K-Ras-induced distal lung adenocarcinoma. Proc Natl Acad Sci U S A 109, 4910–4915 (2012). [PubMed: 22411819]
34. Sutherland KD et al. , Multiple cells-of-origin of mutant K-Ras-induced mouse lung adenocarcinoma. Proc Natl Acad Sci U S A 111, 4952–4957 (2014). [PubMed: 24586047]
35. Lin C et al. , Alveolar type II cells possess the capability of initiating lung tumor development. PLoS One 7, e53817 (2012). [PubMed: 23285300]
36. Spella M et al. , Club cells form lung adenocarcinomas and maintain the alveoli of adult mice. Elife 8 (2019).

37. Martínez-Reyes I et al. , Mitochondrial ubiquinol oxidation is necessary for tumour growth. Nature 585, 288–292 (2020). [PubMed: 32641834]
38. Frank M, Kemler R, Protocadherins. Curr Opin Cell Biol 14, 557–562 (2002). [PubMed: 12231349]
39. Tang X et al. , Protocadherin 10 is frequently downregulated by promoter methylation and functions as a tumor suppressor gene in non-small cell lung cancer. Cancer Biomark 12, 11–19 (2012). [PubMed: 23321465]
40. Harada H et al. , Prognostic signature of protocadherin 10 methylation in curatively resected pathological stage I non-small-cell lung cancer. Cancer Med 4, 1536–1546 (2015). [PubMed: 26276761]
41. Tsai PC et al. , Smoking induces coordinated DNA methylation and gene expression changes in adipose tissue with consequences for metabolic health. Clin Epigenetics 10, 126 (2018). [PubMed: 30342560]
42. Ye M, Li J, Gong J, PCDH10 gene inhibits cell proliferation and induces cell apoptosis by inhibiting the PI3K/Akt signaling pathway in hepatocellular carcinoma cells. Oncol Rep 37, 3167–3174 (2017). [PubMed: 28498423]
43. Yang Y et al. , Protocadherin 10 inhibits cell proliferation and induces apoptosis via regulation of DEP domain containing 1 in endometrial endometrioid carcinoma. Exp Mol Pathol 100, 344–352 (2016). [PubMed: 26970279]
44. Xu Y et al. , PCDH10 inhibits cell proliferation of multiple myeloma via the negative regulation of the Wnt/β-catenin/BCL-9 signaling pathway. Oncol Rep 34, 747–754 (2015). [PubMed: 26081897]
45. Rath E, Moschetta A, Haller D, Mitochondrial function - gatekeeper of intestinal epithelial cell homeostasis. Nat Rev Gastroenterol Hepatol 15, 497–516 (2018). [PubMed: 29844587]
46. van Roy F, Beyond E-cadherin: roles of other cadherin superfamily members in cancer. Nat Rev Cancer 14, 121–134 (2014). [PubMed: 24442140]
47. Kim SY, Yasuda S, Tanaka H, Yamagata K, Kim H, Non-clustered protocadherin. Cell Adh Migr 5, 97–105 (2011). [PubMed: 21173574]
48. Yang Y et al. , E3 ubiquitin ligase Mule ubiquitinates Miz1 and is required for TNFalpha-induced JNK activation. Proc Natl Acad Sci U S A 107, 13444–13449 (2010). [PubMed: 20624960]
49. Yi J et al. , DNA damage-induced activation of CUL4B targets HUWE1 for proteasomal degradation. Nucleic Acids Res 43, 4579–4590 (2015). [PubMed: 25883150]
50. Liu F et al. , CRL4B(RBBP7) targets HUWE1 for ubiquitination and proteasomal degradation. Biochem Biophys Res Commun 501, 440–447 (2018). [PubMed: 29738775]
51. Sarantopoulos J et al. , Phase I Study of the Investigational NEDD8-Activating Enzyme Inhibitor Pevonedistat (TAK-924/MLN4924) in Patients with Advanced Solid Tumors. Clin Cancer Res 22, 847–857 (2016). [PubMed: 26423795]
52. Do-Umehara HC et al. , Suppression of inflammation and acute lung injury by Miz1 via repression of C/EBP-δ. Nat Immunol 14, 461–469 (2013). [PubMed: 23525087]
53. Sanjana NE, Shalem O, Zhang F, Improved vectors and genome-wide libraries for CRISPR screening. Nat Methods 11, 783–784 (2014). [PubMed: 25075903]
54. Yang J et al. , Identification of the SARS-CoV-2 Entry Receptor ACE2 as a Direct Target for Transcriptional Repression by Miz1. Front Immunol 12, 648815 (2021). [PubMed: 34305888]
55. Helmin KA et al. , Maintenance DNA methylation is essential for regulatory T cell development and stability of suppressive function. J Clin Invest 10.1172/jci137712 (2020).
56. Győrffy B, Surowiak P, Budczies J, Lánczky A, Online survival analysis software to assess the prognostic value of biomarkers using transcriptomic data in non-small-cell lung cancer. PLoS One 8, e82241 (2013). [PubMed: 24367507]

Highlights

Lung cancer is the leading cause of cancer-related death worldwide. NSCLC is the most common form of lung cancer, with KRAS being the most frequently mutated oncogene. Development of therapies to directly target KRAS function remains challenging. Alternative strategies aim at targeting codependent vulnerabilities or synthetic lethal partners that are essential in the context of oncogenic KRAS. Our data show that oncogenic KRAS upregulates Miz1, which in turn represses Pcdh10, resulting in increased tumor cell proliferation and promotion of lung tumorigenesis. Importantly, targeting Miz1 has marginal effect on non-tumorigenic cells or WT KRAS human NSCLC cells. Our data suggest that Miz1 promotes tumorigenesis in MT KRAS NSCLC through repression of Pcdh10 and thus reveal therapeutic potentials.

Significance

Lung cancer is the leading cause of cancer-related death worldwide. NSCLC is the most common form of lung cancer, with KRAS being the most frequently mutated oncogene. Development of therapies to directly target KRAS function remains challenging. Alternative strategies aim at targeting codependent vulnerabilities or synthetic lethal partners that are essential in the context of oncogenic KRAS (1, 2). Our data show that oncogenic KRAS upregulates Miz1, which in turn represses Pcdh10, resulting in increased tumor cell proliferation and promotion of lung tumorigenesis. Importantly, targeting Miz1 has marginal effect on non-tumorigenic cells or WT KRAS human NSCLC cells. Our data suggest that Miz1 promotes tumorigenesis in MT KRAS NSCLC through repression of Pcdh10 and thus reveal therapeutic potentials.

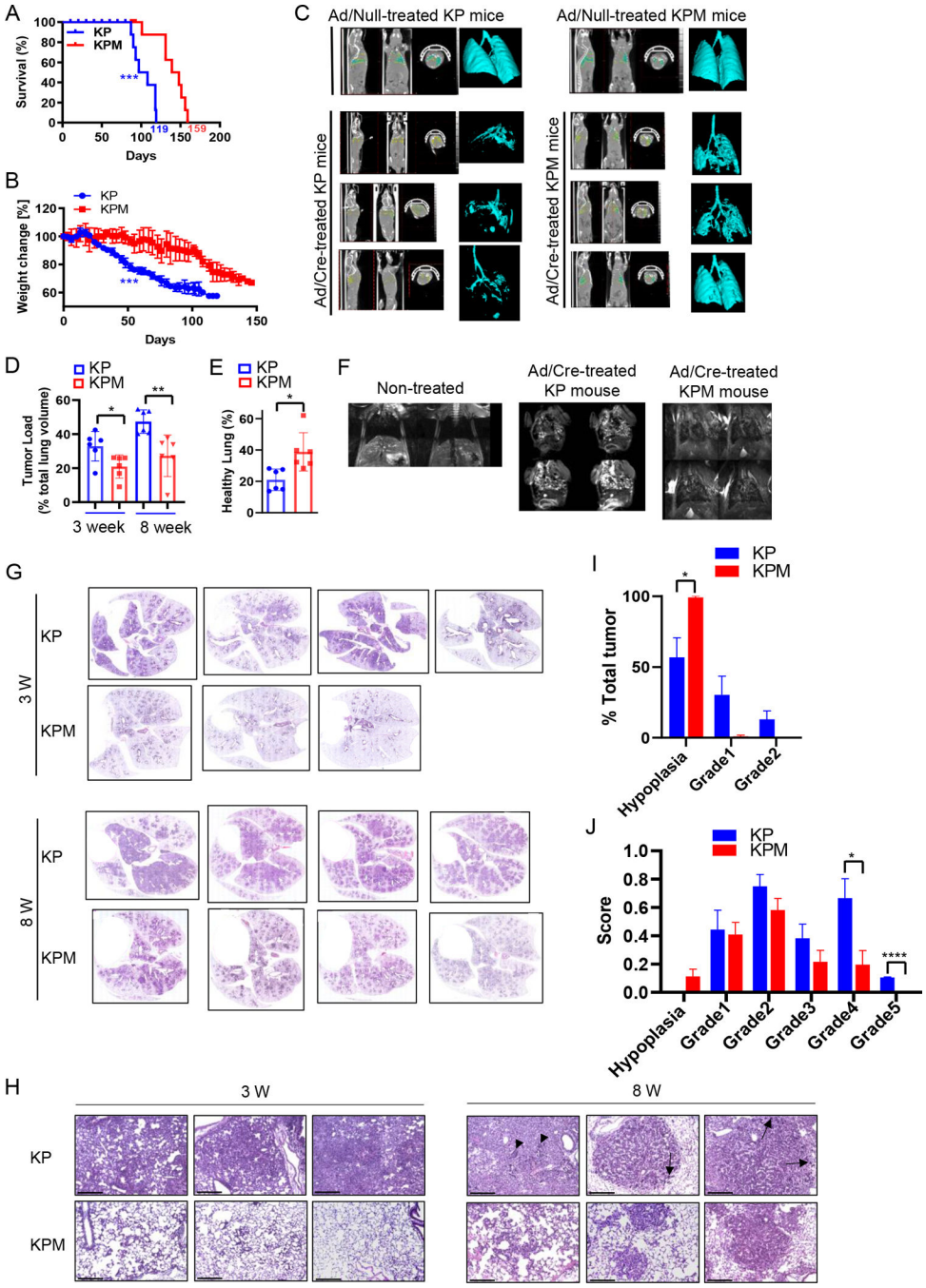

Figure 1. Loss of function of Miz1 inhibits tumor growth and progression in KRAS-driven mouse lung cancer model.

Ad/Cre was i.t. instilled into KP or KP mice. (**A,B**) Mortality rate (**A**) and weight loss (**B**) of the mice were monitored. n=8. (**C**) micro-CT scan of Ad/null- or Ad/Cre-treated KP or KPM mice at 8 weeks post Ad infection. n=6. (**D,E**) Tumor loads (**D**) or healthy lung area percentage (**E**) quantified by micro-CT of Ad/Cre-treated KP or KPM mice at 3- or 8-weeks post Ad/Cre infection. n=6. (**F**) MRI images of non-treated or Ad/Cre-treated KP or KPM mice. (**G,H**) TissueGnostics of whole lung (**G**) or sectional lung histology (**H**) by

hematoxylin and eosin staining from Ad/Cre-treated KP or KPM mice at 3- or 8-weeks post Ad/Cre infection. n=3–4. Arrows: aberrant mitoses. Arrow heads: tumor giant cells. Scale bars: 100 μm. (**I,J**) Tumor grades of Ad/Cre-treated KP or KPM mice at 3- (**I**) or - weeks (**J**) post Ad/Cre infection analyzed by HALO software. n=3–4. *, $p < 0.05$; **, $p < 0.01$; ***, $p < 0.001$. For all panels, values represent the mean ± SEM.

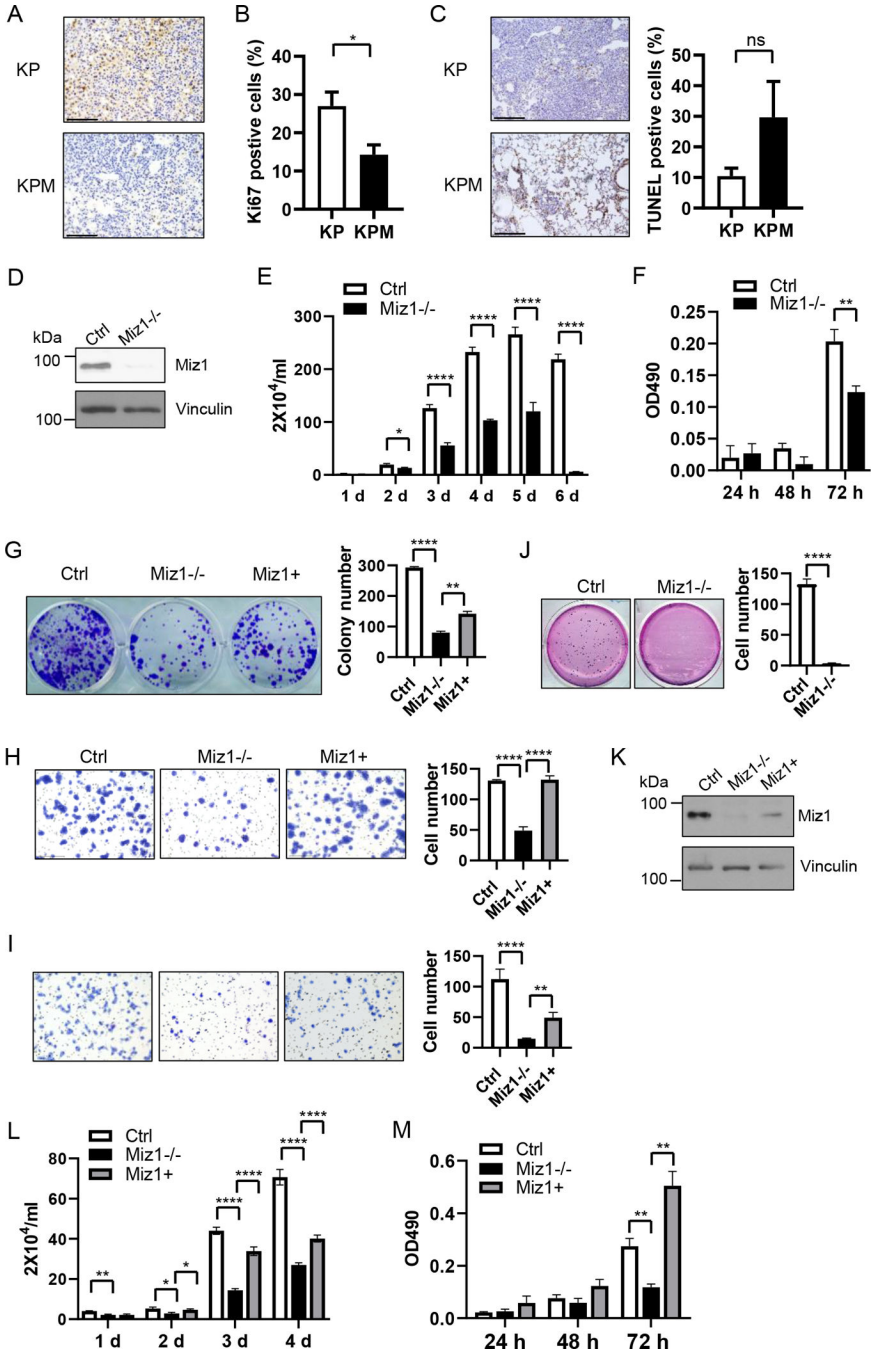

Figure 2. Miz1 knockout reduces cell proliferation, clonogenicity, anchorage-independent growth, migration, and invasion in murine KRAS-mutant lung tumor cells.

(**A-C**) Ki67 staining (**A**) and quantification analyzed by HALO software (**B**), and TUNEL staining and quantification analyzed by HALO software (**C**) of Ad/Cre-treated KP or KPM mice at 8-weeks post Ad/Cre infection. n=7. Positive staining is brown/dark brown, and the nuclei are stained blue. Scale bars: 100 μm. (**D**) Miz1 western blot confirmed Miz1 KO in KP cells. (**E-M**) Growth assay (**E,L**), MTS assay (**F,M**), colony assay (**G**), migration assay (**H**), invasion assay (**I**), and soft agar assay (**J**) in control, Miz1 KO, and/or Miz1+ (Miz1

KO KP cells with Miz1 re-introduction) KP cells. (**K**) Miz1 western blot confirmed Miz1 re-introduction in Miz1 KO KP cells (Miz1+). For **E-J, L-M**, n=3–6. *, $p < 0.05$; **, $p < 0.01$; ****, $p < 0.0001$; ns, not significant. For all panels, values represent the mean ± SEM.

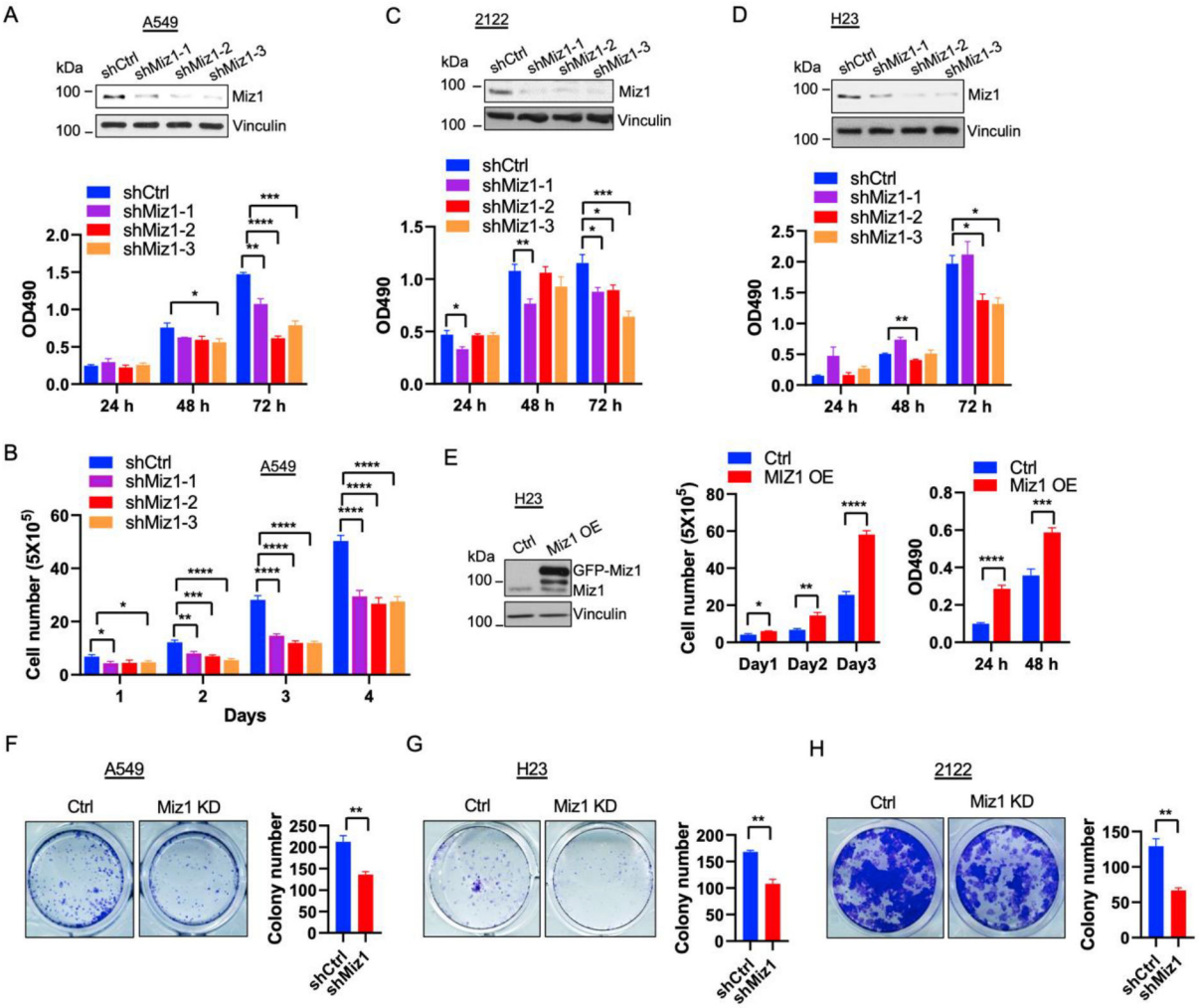

Figure 3. Silencing of Miz1 also reduces cell proliferation and clonogenicity in KRAS-mutant human lung cancer cells.

(**A,B**) MTS (**A**) and growth assays (**B**) of control and Miz1 KD A549 cells. (**C,D**) MTS assay of control and Miz1 KD NCI-2122 (**C**) and NCI-H23 cells (**D**). (**E**) Growth and MTS assays of control and Miz1-overexpressing (Miz1 OE) NCI-H23 cells. (**F-H**) Colony assay and quantification of control and Miz1 KD A549 (**F**), NCI-H23 (**G**), and NCI-2122 cells (**H**). For **A-H**, n=3–5. *, $p < 0.05$; **, $p < 0.01$; ***, $p < 0.001$; ****, $p < 0.0001$. For all panels, values represent the mean ± SEM.

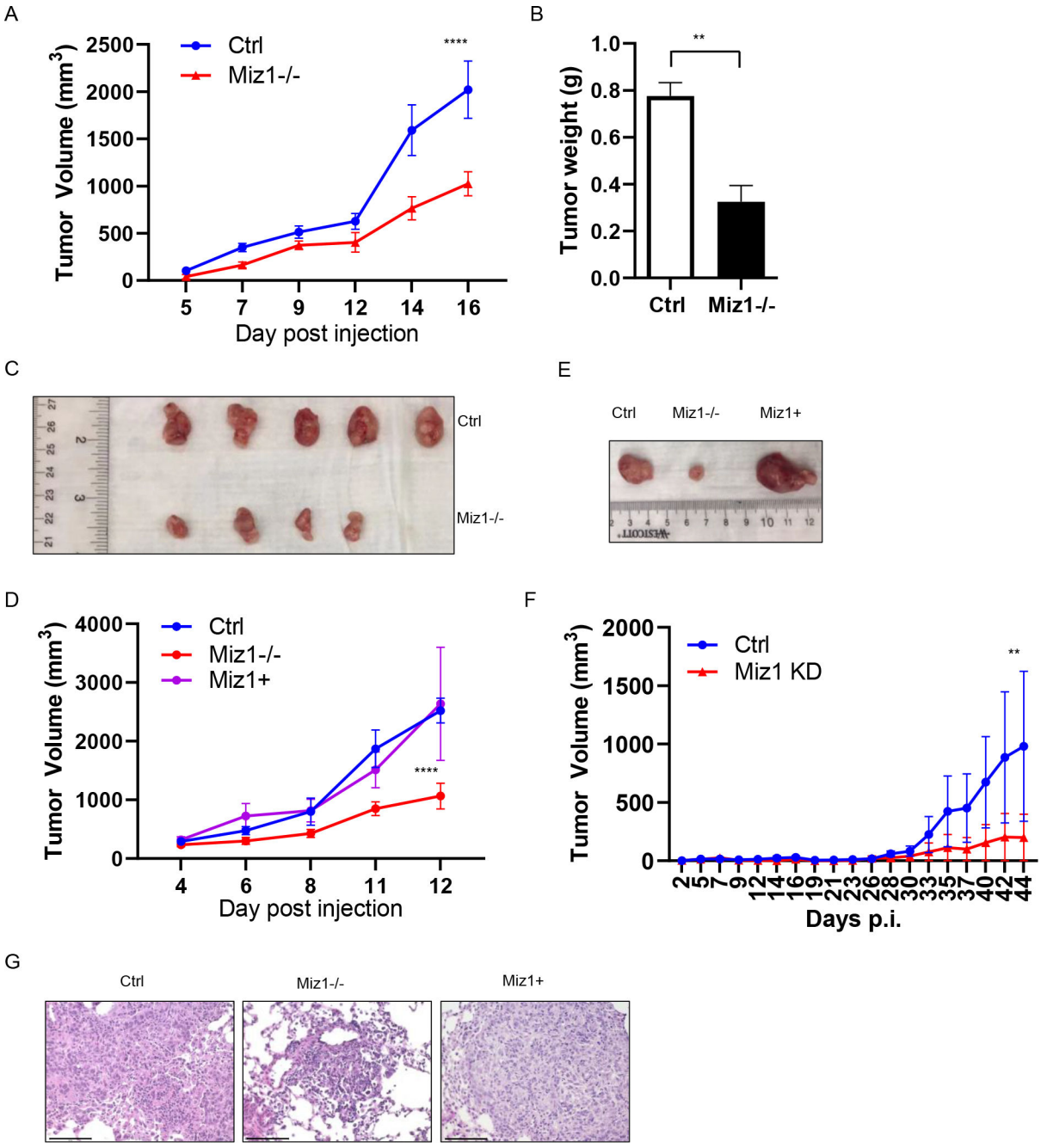

Figure 4. Miz1 knockout or knockdown suppresses tumor growth in xenograft or allograft mouse models.

(**A-C**) Tumor volume (**A**), tumor weight (**B**) and images of dissected tumors (**C**) from allograft tumors derived from control or Miz1 KO KP cells in nude mice. n=4–5. (**D,E**) Tumor volume (**D**) and representative images of dissected tumors (**E**) in allograft tumors derived from control, Miz1 KO, or Miz1+ KP cells in nude mice. n=5–6. (**F**) Tumor volume of xenograft tumors derived from control or Miz1 KD NCI-H23 cells in nude mice. n=4–5. (**G**) Histology of lung sections containing allograft tumors derived from orthotopic lung

transplantation of control, Miz1 KO, or Miz1+ KP cells in C57Bl6 mice. Scale bars: 100 μm. **, $p < 0.01$; ****, $p < 0.0001$. For all panels, values represent the mean ± SEM.

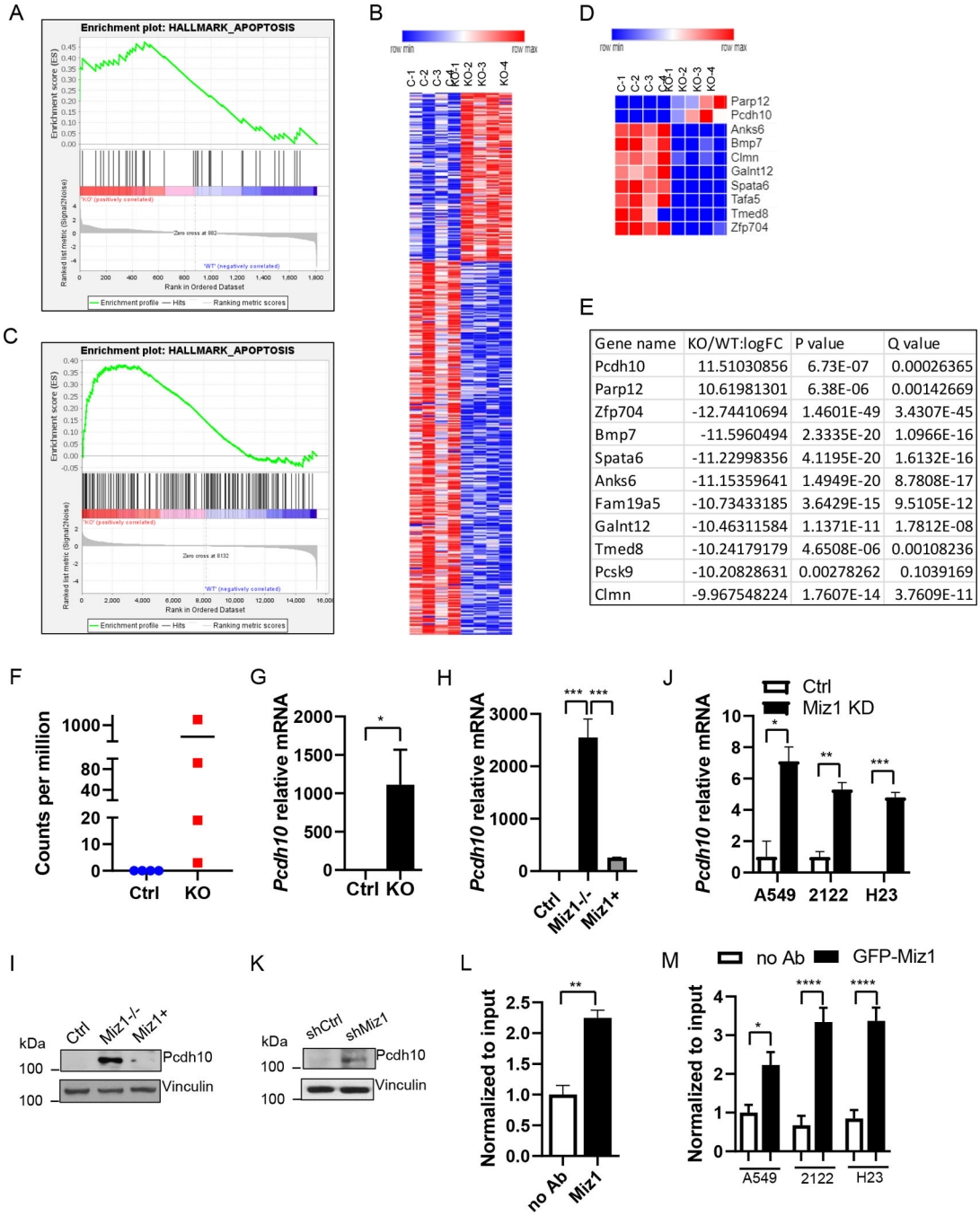

Gene name	KO/WT:logFC	P value	Q value
Pcdh10	11.51030856	6.73E-07	0.00026365
Parp12	10.61981301	6.38E-06	0.00142669
Zfp704	-12.74410694	1.4601E-49	3.4307E-45
Bmp7	-11.5960494	2.3335E-20	1.0966E-16
Spata6	-11.22998356	4.1195E-20	1.6132E-16
Anks6	-11.15359641	1.4949E-20	8.7808E-17
Fam19a5	-10.73433185	3.6429E-15	9.5105E-12
Galnt12	-10.46311584	1.1371E-11	1.7812E-08
Tmed8	-10.24179179	4.6508E-06	0.00108236
Pcsk9	-10.20828631	0.00278262	0.1039169
Clmn	-9.967548224	1.7607E-14	3.7609E-11

Figure 5. Pcdh10 is the top upregulated gene by Miz1 knockout in KRAS-mutant murine lung tumor cells and Miz1 binds to and represses the *Pcdh10* promoter.

(**A**) GSEA showing enrichment plot of the gene set of "Apoptosis" from upregulated proteins in the lungs of Ad/Cre-treated KPM compared to those of Ad/Cre-treated KP mice as analyzed by proteomics. n=3. (**B**) Heatmap of differentially expressed genes in Miz1 KO KP cells compared to control KP cells. n=4. (**C**) GSEA showing enrichment plot of the gene set of "Apoptosis" from differentially expressed genes in Miz1 KO KP cells compared to control KP cells as analyzed by RNA-seq. n= 4. (**D**) Heatmap of top

10 differentially expressed genes in Miz1 KO KP cells compared to control KP cells. n= 4. (**E**) Log-transformed fold change (logFC), p value and q value of top 10 differentially expressed genes in Miz1 KO KP cells compared to control KP cells. n= 4. (**F**) mRNA expression (unnormalized; counts per million) of *Pcdh10* in control and Miz1 KO KP cells. n= 4. (**G**) *Pcdh10* mRNA expression in different clones of control and Miz1 KO KP cells analyzed by qRT-PCR. n= 6. (**H,I**) *Pcdh10* mRNA (**H**) and protein expressions (**I**) in control, Miz1 KO, or Miz1+ KP cells. (**J**) *PCDH10* mRNA expression in control and Miz1 KD A549/NCI-2122/NCI-H23 cells. (**K**) PCDH10 protein expression in control and Miz1 KD A549 cells. (**L,M**) Miz1 binding on the *Pcdh10* promoter analyzed by ChIP in KP cells (**L**) or Miz1-overexpressing (Miz1 OE) A549/NCI-2122/NCI-H23 cells (**M**). *, $p < 0.05$; ***, $p < 0.001$. For all panels, values represent the mean ± SEM.

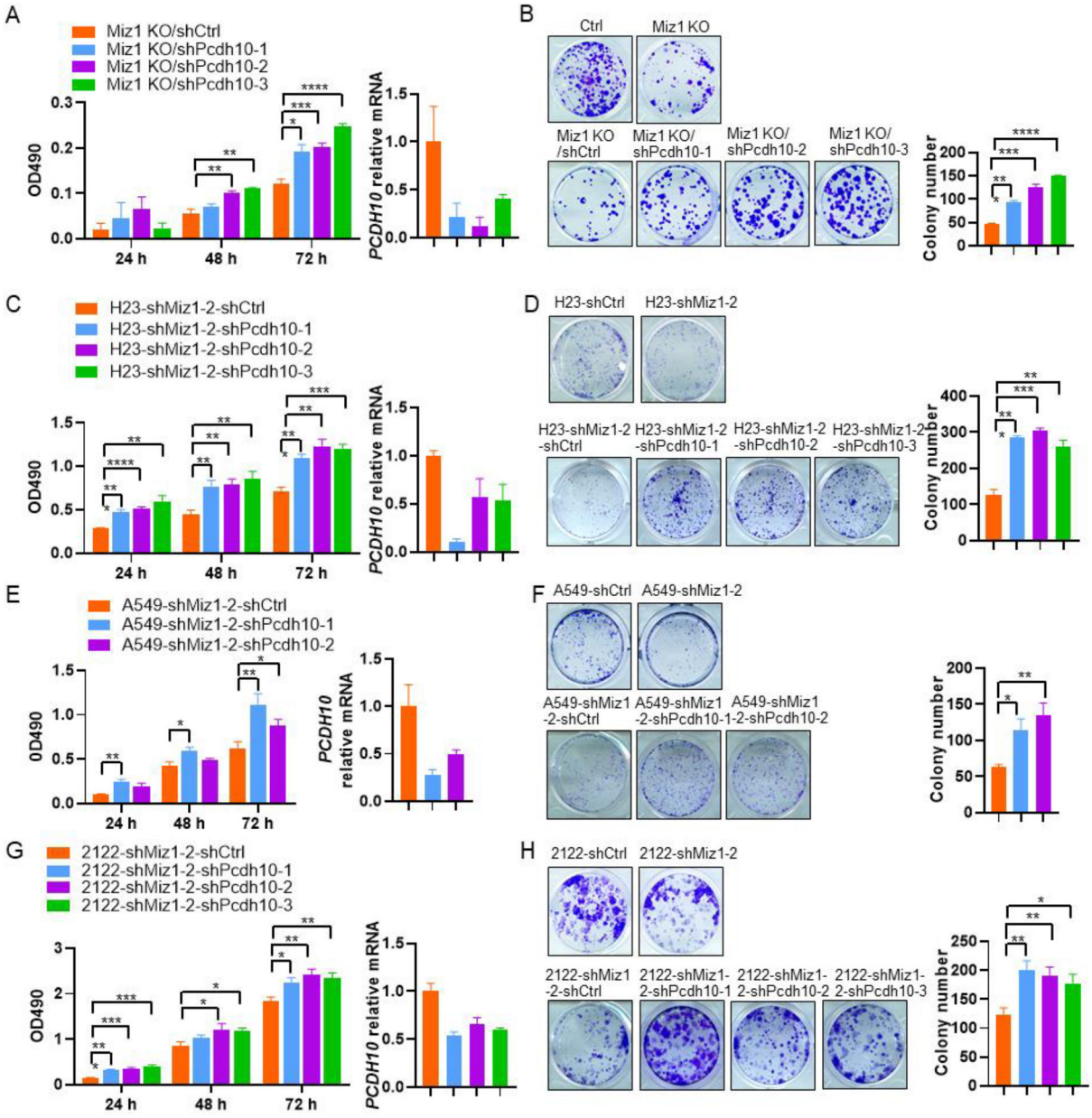

Figure 6. Silencing of Pcdh10 rescues cell proliferation and clonogenicity in Miz1-knockout or -knockdown KRAS-mutant mouse and human lung tumor cells.

(**A-H**) MTS assay (**A,C,E,G**) and colony formation (**B,D,F,H**) in control KP or A549/NCI-H23/NCI-2122, or Miz1 KO KP or Miz1 KD A549/NCI-H23/NCI-2122, or Pcdh10 KD/ Miz1 KO KP or Pcdh10 KD/Miz1 KD A549/NCI-H23/NCI-2122 or their corresponding control Miz1 KO KP or Miz1 KD A549/NCI-H23/NCI-2122 cells. n=3–5. *, $p < 0.05$; **, $p < 0.01$; ***, $p < 0.001$; ****, $p < 0.0001$. For all panels, values represent the mean ± SEM.

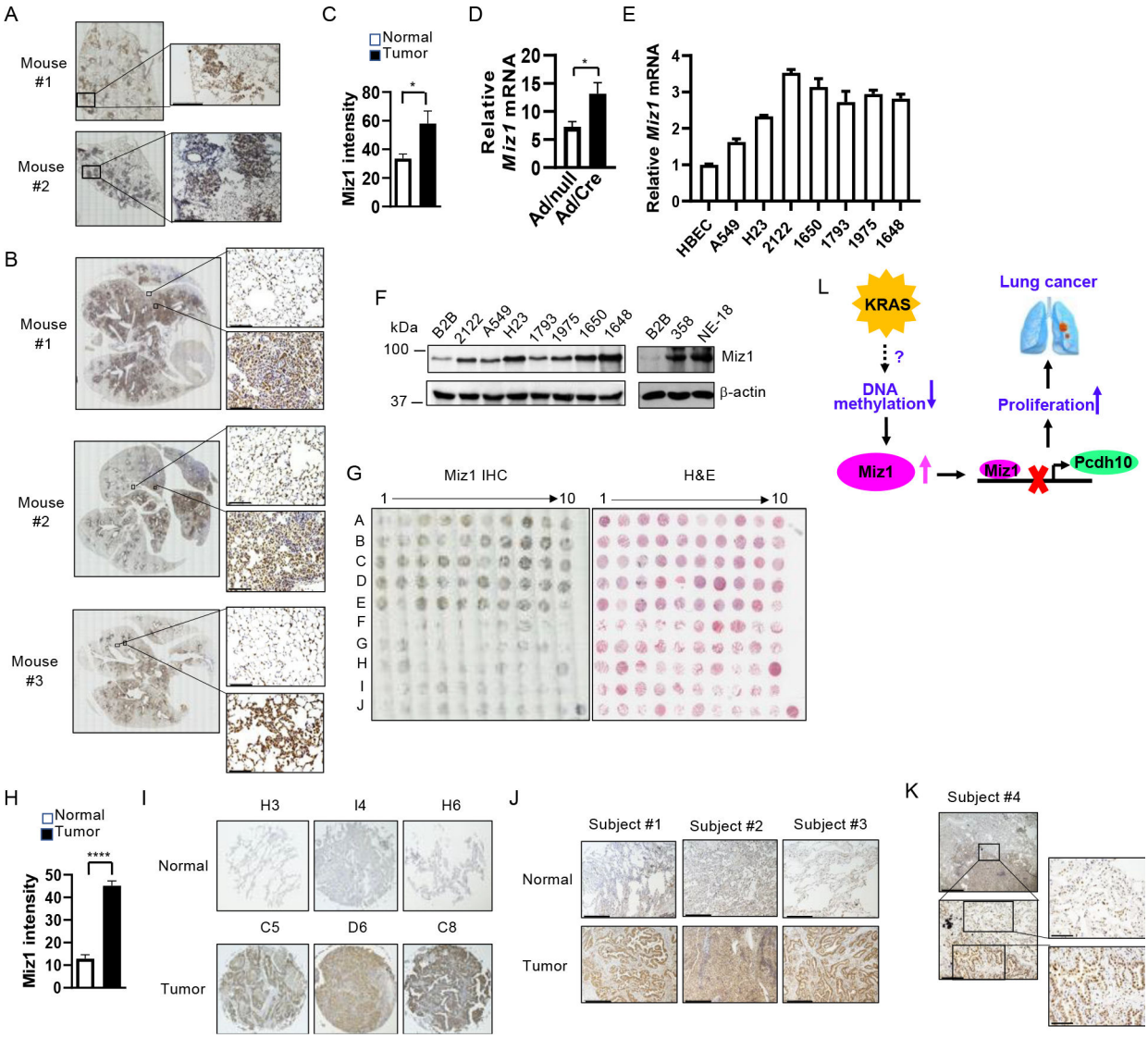

Figure 7. Miz1 is upregulated in KRAS-mutant murine lung tumors and human NSCLC cell lines and primary tumors.

(**A,B**) Miz1 IHC of Ad/Cre-treated $Kras^{LSL\text{-}G12D/+}$ (**A**) or KP mice (**B**). Positive staining is brown/dark brown. The nuclei are stained blue. (**C**) Quantification of Miz1 IHC in tumor tissues and normal tissues from Ad/Cre-treated KP mice. n=8. (**D**) Miz1 mRNA expression in Ad/null- or Ad/Cre-treated AT2 cells isolated from KP mice. AT2 were isolated using antibody-based affinity purification with CD45 negative selection and EpCAM positive selection. (**E,F**) Miz1 mRNA (**E**) and protein expressions (**F**) in NSCLC cell lines. (**G,H**) Miz1 IHC (**G**) and quantification (**H**) of tumor tissues and paired normal tissues from lung adenocarcinoma TMA. In F, H&E staining was shown in the right panel. n=48. (**I**) Representative images of Miz1 IHC from paired tumor/normal samples of lung adenocarcinoma TMA in **G**. (**J,K**) Representative images of Miz1 IHC in paired tumor/normal samples of NSCLC from the UIC Medical Center. Scale bars: 100 μm. Note: Positive staining is brown/dark brown, and the nuclei are stained blue. *, $p < 0.05$; ****, $p < 0.0001$. For all panels, values represent the mean ± SEM. (**L**) A diagram showing that oncogenic

KRAS upregulates Miz1, which in turn represses Pcdh10, resulting in increased tumor cell proliferation and promotion of lung tumorigenesis.